MCNC MEMS TECHNOLOGY APPLICATIONS CENTER

MEMS Sensors Commercial Technology Insertion Program (CTIP)

Final Report

Reporting Period May 1, 1997-June 30, 1998

Federal Contract: N0001A-97-1-0660
MCNC Contract: C97-5113-820

Prepared by: Robert L. Wood
MCNC MEMS Technology Applications Center
3021 Cornwallis Road
Research Triangle Park NC 27709
919-248-9284
rwood@mcnc.org

REPORT DOCUMENTATION PAGE

Form Approved
OMB No. 0704-0188

1. AGENCY USE ONLY *(Leave blank)*	2. REPORT DATE	3. REPORT TYPE AND DATES COVERED
	10-6-98	FINAL 5/1/97-6/30/98

4. TITLE AND SUBTITLE
MEMS Sensors Commercial Technology Insertion Program (CTIP)

5. FUNDING NUMBERS
Grant
Federal Number:
N00014-97-1-0660

6. AUTHOR(S)
Robert L. Wood

7. PERFORMING ORGANIZATION NAME(S) AND ADDRESS(ES)
MCNC
3021 Cornwallis Road
Research Triangle Park, NC 27709

8. PERFORMING ORGANIZATION REPORT NUMBER
C97-5113-820

9. SPONSORING/MONITORING AGENCY NAME(S) AND ADDRESS(ES)
Office of Naval Research
ONR 254: Joyce W. Keller
800 North Quincy Street
Arlington, VA 22217-5660

10. SPONSORING/MONITORING AGENCY REPORT NUMBER

11. SUPPLEMENTARY NOTES
N/A

12a. DISTRIBUTION/AVAILABILITY STATEMENT
NO LIMITATIONS

12b. DISTRIBUTION CODE

13. ABSTRACT *(Maximum 200 words)*

This report summarizes results of efforts under the MEMS Sensor Commercial Technology Program (CTIP) from 5/97 through 6/98. The program was established to assist Naval Surface Warfare Center (NSWC) Indian Head Division in procurement, characterization, and fabrication of COTS sensors applicable to the SMTD S & A system as well as general DOD needs. Highlights of major accomplishments are provided.

14. SUBJECT TERMS
MEMS, COTS, Sensors

15. NUMBER OF PAGES

16. PRICE CODE

17. SECURITY CLASSIFICATION OF REPORT	18. SECURITY CLASSIFICATION OF THIS PAGE	19. SECURITY CLASSIFICATION OF ABSTRACT	20. LIMITATION OF ABSTRACT
N/A	N/A	N/A	SAR

NSN 7540-01-280-5500

Standard Form 298 (Rev. 2-89)
Prescribed by ANSI Std. Z39-18
298-102

MEMS Sensor Commercial Technology Insertion Program
Final Report on Activities through June, 1998

Introduction

This report summarizes the results of efforts performed under the MEMS Sensor Commercial Technology Insertion Program (CTIP) from May 1997 through June 1998. This program was established to assist Naval Surface Warfare Center (NSWC), Indian Head Division, in procurement, characterization, and fabrication of MEMS-based COTS sensors applicable to the SMTD S&A system as well as general DoD needs. The work was performed by several organizations, with MCNC acting as program ombudsman. The major objectives were as follows:

- Coordinate with NSWC in selection and procurement of COTS sensors for Phase 1 and 2 environmental evaluations to include temperature, vibration, and shock sensitivity. These sensors will support SMTD-specific goals as well as general DoD needs.
- Help expand COTS database of domestic and foreign suppliers
- Engineering support of testing and analysis of COTS sensors and associated system requirements.
- Fabrication of HIMEMS-based S&A sensors and devices in collaboration with the former TRP Alliance. This supports NSWC's Phase 3-5 SMTD system prototype objectives.
- Fabrication of IEP Group commercial flow sensors for use in underwater and air-launch applications.

Participating groups in this program include:

- NSWC Indian Head Division, Indian Head, MD
- MCNC, Research Triangle Park, NC
- Oak Ridge National Labs, Oak Ridge, TN
- Boeing Co. Inc. (formerly McDonnell Douglas), St. Louis, MO
- Center for Advanced Microstructures and Devices (LSU CAMD), Baton Rouge, LA
- IEP Group Inc., Raleigh, NC

This report provides brief highlights of major accomplishments achieved under the CTIP program. Detailed reports on some aspects of this work are enclosed, and additional technical reports on specific topics are available through MCNC.

Environmental Testing of COTS Sensors (NSWC with MCNC)

MCNC procured COTS sensors for evaluation in CTIP Phase I and Phase II environmental tests. Sensors include MEMS accelerometers, pressure sensors, and an RF transponder. The primary goal of the Phase I effort of the CTIP MEMS project was

to assess the viability of using various Commercial Off-The-Shelf (COTS) MEMS devices in military applications (reference 1). Vendors with existing or near-term offerings of MEMS sensors were identified, and selected devices procured for Phase I environmental testing, including vibration, shock, and thermal shock test profiles. Pressure sensors were functionally tested to verify proper performance after each environmental test. For the transponders and magnetic sensors, the performance was verified at the completion of all the tests.

Inertial and pressure sensing transducers were obtained from five MEMS sensor vendors. Vibration tests were designed to encompass typical aircraft, ship, and transportation environments. Profiles consisted of sinusoidal as well as random spectrum tests, with vibrations in the 20-2000Hz range up to 10 grms, 3-axis, 30 minutes each axis, under hot, ambient, and cold conditions. Sensors were also subjected to mechanical shock ranging from 60g for 10 ms to 5000g for 0.5ms. Tests were performed at ambient temperature conditions as well as two temperature extremes—a high temperature extreme of +160°F and a low of -65°F.

In addition, an RF Microstamp transponder demonstration kit was purchased from Micron Communications. The transponders are a radio frequency identification device with a single chip consisting of a passive transponder and controller that provides a 2.44 GHz signal with a typical range of 15 feet. This system has potential applications in weapons cookoff remote sensing.

All the MEMS devices tested met or exceeded the manufacturer specifications. Most devices not only met these specifications, but also survived a broad spectrum of generic military environments well beyond the claimed performance. The feasibility and utility of performing a generic survivability-testing program was also successfully demonstrated. The tests performed indicated that all of the devices were viable candidates for potential military applications.

The inertial sensors purchased by MCNC and tested in CTIP environmental testing are strong candidates for insertion into several military applications. These include, NSWC underwater MEMS S&A, Army Research Laboratory High-g telemetry units and Eglin Air-Force Base High-g penetration fuzing. The pressure sensors procured by MCNC also have application in on-going military programs. These include use in underwater weapon S&A and fuzing.

Differential Pressure Sensor (NSWC)

A commercially available (Honeywell) MEMS differential pressure sensor was adapted into an NSWC-designed pitot flow configuration for use as a water flow sensor. Lab tests demonstrated good sensitivity between 50°F and 70°F, with little sensitivity change up to 350 psi. The device was operable after a survivability test up to 700 psi. Two sea-run tests incorporating this sensor were completed at NSWC in June 1998. Data analysis shows excellent shear-stress correlation between the flow simulator and sea-run data. These results supported downselect of this device as the baseline S&A flow sensor for SMTD and other torpedo applications, superceding original plans calling for use of the IEP flow sensor.

In FY 99, NSWC Indian Head will insert the differential pressure sensor into torpedo sea-run tests and apply the sensor as a integral part of the MEMS S&A sea-run test demonstration.

Dynamic Characterization of MEMS Sensors (Boeing with NSWC)

Components of NSWC's MEMS-based S&A system were subjected to force-displacement testing and dynamic response characterization (reference 2). This effort was necessary to support continued evolution of SMTD component design and sensitivity to environmental vibration. Novel techniques developed at Boeing Co. (formerly McDonnell Douglas) for direct mechanical measurement of MEMS microspring stiffness were used in this study. A laser vibrometer was used for dynamic response. Slider/barrier components fabricated by the LIGA technique were characterized. These structures are intended to respond, under microactuator control, to input provided by environmental sensors that unlock the slider and arm the fireset. The slider barrier is suspended on microsprings and travels over a range of hundreds of microns during arming.

It is imperative to understand the stiffness and linearity of the springs restraining the slider against the microactuators, and to determine their resonant frequencies and damping characteristics in order to estimate threshold environmental vibration tolerance. Tests employed at Boeing demonstrated excellent reproducibility and consistency, and were able to measure spring stiffness constants as low as 0.009 milliNewtons/micron. Good spring linearity was confirmed. Resonant frequency characterization provided useful information on frequency, mode description, and damping/Q of the slider/barriers. Results were used to validate designs for next-generation S&A components in NSWC's SMTD program.

Hydrolock Design and Modeling (MCNC with NSWC)

This effort was directed toward adaptation of existing MEMS hydrostat designs for measurement of water flow, rather than simple static pressure. Such an approach would permit integration of the flow sensor at the MEMS S&A chip level, resulting in system simplification and further miniaturization. The concept is based on a proven MEMS thermal actuator to drive a locking element, and make use of forced convection temperature gradient to alter the equilibrium position of the actuator. Under the selected flow conditions, displacement of the actuator would result in device unlocking at the appropriate weapon velocity.

Such a device was designed, and a thermomechanical simulation of its performance was conducted. It was determined that forced convection at a target flow velocity of 9.1 m/sec could produce a temperature differential of 225°K/W compared to no flow. This differential could in principal be used to drive the thermal actuator with sufficient displacement to unlock the S&A device. However, it was found that a high degree of thermal isolation required between the heater and the surrounding device could not be easily realized in an integrated process. It would also be difficult to protect the device from the liquid environment while still achieving good thermal coupling between

the liquid and the sensor. For these reasons, the hydrolock concept was not pursued further.

United Micromachines Sensor Evaluation (NSWC)

Shear stress flow sensors developed at UCLA and Caltech, and licensed to United Micromachines, were adapted to measurement of seawater flow. These sensors are intended for application in measuring flow induced shear stresses over advanced aircraft wings. The sensor relies on a shear stress gradient produced by forced convection, which can be detected electrically in thermally isolated silicon resistor structures. Flexible versions of these devices were mounted on curved sections of a 12-inch diameter torpedo section and tested in NSWC's flow tunnel. Sensitivity was shown to be good up to 50 ft/sec (maximum available in tunnel). No sensor failed during testing, including a 30-minute high-speed endurance test. Additional development is required for device ruggedization, improvement of corrosion resistance and temperature compensation.

The MCNC-procured United Micromachines sensors established this type of sensor as a viable device for water flow sensing in torpedo application. In FY-99, a DAPRA sponsored test program conducted by NSWC Indian Head will further explore the survivability and ruggedness of the device in laboratory testing.

G-Sensor Spin Testing (Oak Ridge National Lab with NSWC)

A spin table coupled with strobed video microscopy was used at ORNL for observing the displacement and latching behavior of MEMS g-sensors made by MCNC (reference 3). These devices, fabricated via LIGA, are designed to function as threshold acceleration sensors in the SMTD torpedo S&A. A seismic mass suspended by microsprings is deflected toward, and captured by, a mechanical latch under launch acceleration. This completes one of several unlocking events in the S&A. Tests were setup to evaluate sensor deflection *versus* acceleration up to 120 g, and to record the acceleration required to cause device latching. The stroboscopic microscope setup proved very useful in visualizing MEMS devices in action. Results show that the latches require redesign to achieve more consistent locking action—they did not always latch at the same acceleration. Unlatching the latched sensors sometimes resulted in plastic deformation of the latch beams. Suspension springs were found to provide good linearity. Results from these tests have been used to improve designs in current generation g-sensors now being fabricated for NSWC.

The G-sensors testing under the ORNL efforts MCNC CTIP, established a sound methodology for testing current and future MEMS g-sensors deigns.

HIMEMS Fabrication (MCNC, CAMD, and IEP with NSWC)

The former TRP HIMEMS Alliance continued to support LIGA fabrication of S&A component for NSWC under the CTIP program. Two fabrication cycles were completed corresponding to NSWC Phase 3 and Phase 4 prototypes. Sensors fabricated in these runs included the g-sensors tested at ORNL, hydrostat sensors, and the slider/barrier structures evaluated by Boeing as outlined above. Prototype S&A systems

fabricated during this period were successfully tested in sea-run tests performed by NSWC in June of 1998. The HIMEMS sensors fabricated under MCNC CTIP will be further developed and refined through subsequent fabrication runs funded by ONR and DAPRA.

References

1. L.Fan, et al. NSWCIHDIV Report "MEMS Commercial Technology Program (CTIP) - SMTD and Next Generation Underwater Weapons Fuze/Safety and Arming Deivce Sensor Evaluation Program: FY-97 Yearend Report"

2. Characterization of MEMS Devices Under the CTIP Grant to MCNC, Final Report, September 24, 1998, submitted by Edward V.White, The Boing Company (copy enclosed)

3. Boyd M. Evans III, ORNL Report: Report of Work Performed for NSWC Indian Head Division under CTIP Project through MCNC, March 25, 1998 (copy enclosed)

Report of Work Performed
for NSWC Indian Head Division
under CTIP Project through MCNC

Boyd M. Evans III
March 25, 1998

Project Overview

Under the CTIP funding, several tasks were accomplished for the Naval Surface Warfare Center (NSWC), Indian Head Division. The first task that was performed was the development of a testing procedure to spin test g sensors. This procedure was used to conduct two rounds of testing for the NSWC. The procedure is outlined in detail in the following section.

Data analysis of microdevices deflection data was also performed under this project. This analysis consisted of plotting, summarizing, and analyzing data previously gathered for the NSWC. This data is available as a separate report. Also as part of the analysis, several devices were sectioned and viewed under an SEM.

Finally, a considerable amount of effort was spent performing a thermal analysis of a flow sensor for the IEP group. This effort consisted of constructing a three dimensional model of the existing sensor suitable for finite element analysis, transferring the g sensor to the finite element package Pro/Mechanica, and developing a set of boundary conditions and material properties for the model. The model of the existing geometry was run in steady state mode, and later it was adapted for use in a transient mode and was modeled under the conditions of a step energy input to the active area of the anemometer. Some work was done on a follow up model for this project, however resources did not permit analyzing this model. The results of the finite element analysis were delivered to IEP. IEP found the results very helpful and concluded to purchase Pro/Mechanica as funds became available and to perform future modeling at IEP.

Spin Testing Procedure

Overview

The g sensors were tested for latching acceleration by mounting them on a rotating platform and spinning them at several specific rotational velocities. The rotational velocities were calculated to produce specific centrifugal accelerations. The motion of the rotating g sensor was frozen with a strobe light synchronized to the same frequency as the spindle rotation. The motion of the sensor was recorded on video tape through a video microscope.

The acceleration experienced by the g sensor is calculated by dividing the center of gravity velocity squared by the radius of the center of gravity, r, in millimeters. The velocity can be calculated by multiplying the circumference at the CG by the number of rotations per second to get the velocity in mm/sec. The number of g's applied to the center of gravity is determined by dividing the acceleration by the acceleration of gravity in mm/sec^2, as shown in (3). Equation 3 can be rearranged as shown in Equation 4 which relates RPM as a function of desired g load and radius.

(1) $$Velocity = \frac{2\pi rRPM}{60\,\text{sec}/\,\text{min}}$$

(2) $$Acceleration = \frac{Velocity^2}{r} = \frac{4\pi^2 rRPM^2}{3{,}600\,\mathrm{sec}^2/\mathrm{min}^2}$$

(3) $$\#Gs = \frac{Acceleration}{9{,}810\,\mathrm{mm/s}^2} = \frac{4\pi^2 rRPM^2}{(9{,}810\,\mathrm{mm/sec}^2)(3{,}600\,\mathrm{sec}^2/\mathrm{min}^2)}$$

(4) $$RPM = \left[\frac{DesiredG(9{,}810mm/\mathrm{sec}^2)(3{,}600\,\mathrm{sec}^2/\mathrm{min}^2)}{4\pi^2 r}\right]^{1/2}$$

Rotational Platform

The spin testing of g load sensors was performed using a precision single point diamond turning platform. Many of the capabilities of the diamond turning platform are not required for testing g load sensors, however the diamond turning platform has several features which are desirable for testing microdevices. The diamond turning platform is manufactured on an air isolated granite base which provides a vibration free environment for testing microdevices. Also, the diamond turning platform incorporates an air bearing spindle for smooth motion during testing.

Two different diamond turning machines were used for the spin testing of g sensors. The first set of tests was performed on the Precitech Optimum 2800, and the second was performed on the Rank-Pneumo Nanoform 600. The Nanoform 600 was utilized for the second round of testing due to scheduling conflicts. The differences in the two platforms, other than size constraints, are subtle from an optics manufacturing standpoint. The Precitech was manufactured to the same specifications as the Nanoform with the exception of the size optic that the two machines are capable of producing.

Fixturing

A fixture was manufactured on the diamond turning lathe to hold the g sensors during testing. This fixture was manufactured such that it had two stepped areas for easily mounting the g sensors. The sensors were placed against the step to quickly mount them, and ensure that they were placed at the proper radius. All mounting hardware was duplicated to ensure that the assembly was balanced. The sensors were held in place with clamps commonly used to secure mounts on optical tables.

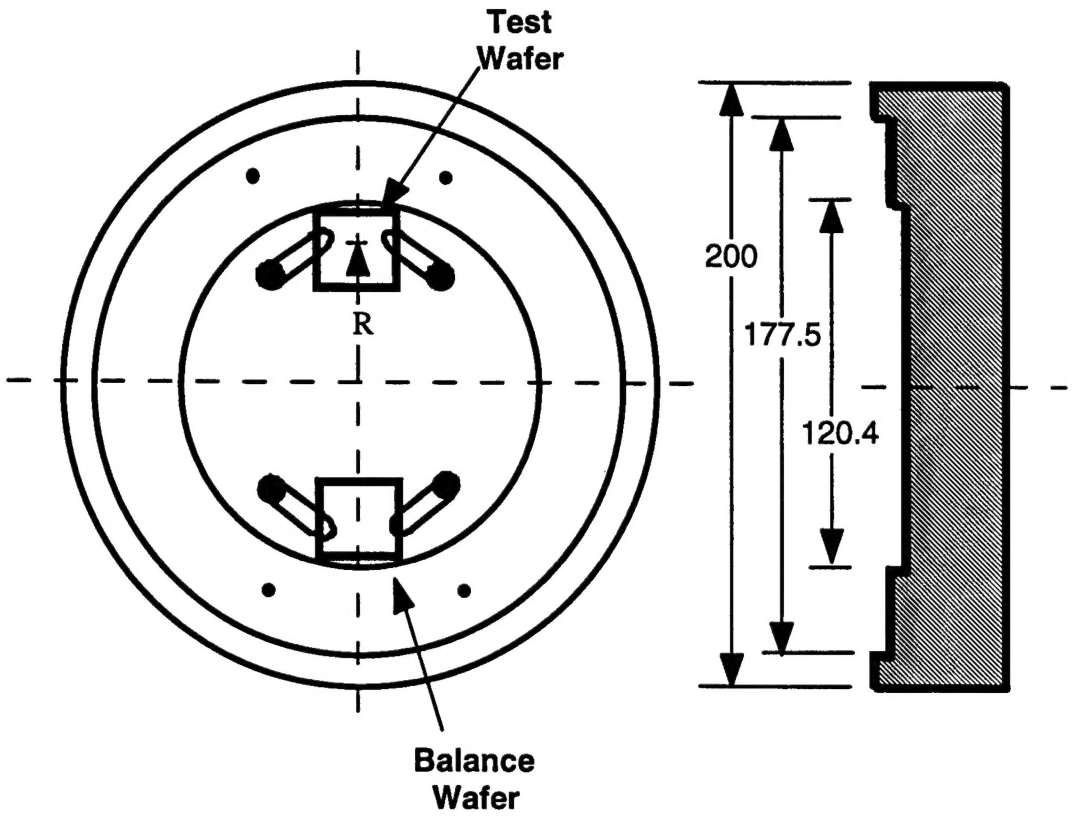

Figure 1: G sensor test fixture. Units in millimeters.

Experimental Setup

The test fixture was mounted on the diamond turning platform's chuck and held in place with vacuum. A CSI Model 404 phototach was used to synchronize the frequency of the spindle rotation to the flashing of the strobe. A piece of reflective tape was attached to the chuck. The phototach detected the reflection of the laser light off of the reflective tape each revolution and emitted a TTL signal.

The strobe was a Monarch Instruments Phaser Strobe. The Phaser strobe accepted the TTL signal from the phototach and was capable of phase adjustment. The phase adjustment was used to adjust the flash such that it occurred at the instant that the g sensor was in front of the video microscope. The strobe also had an output jack for the TTL signal which was utilized to synchronize a second strobe in the second round of testing.

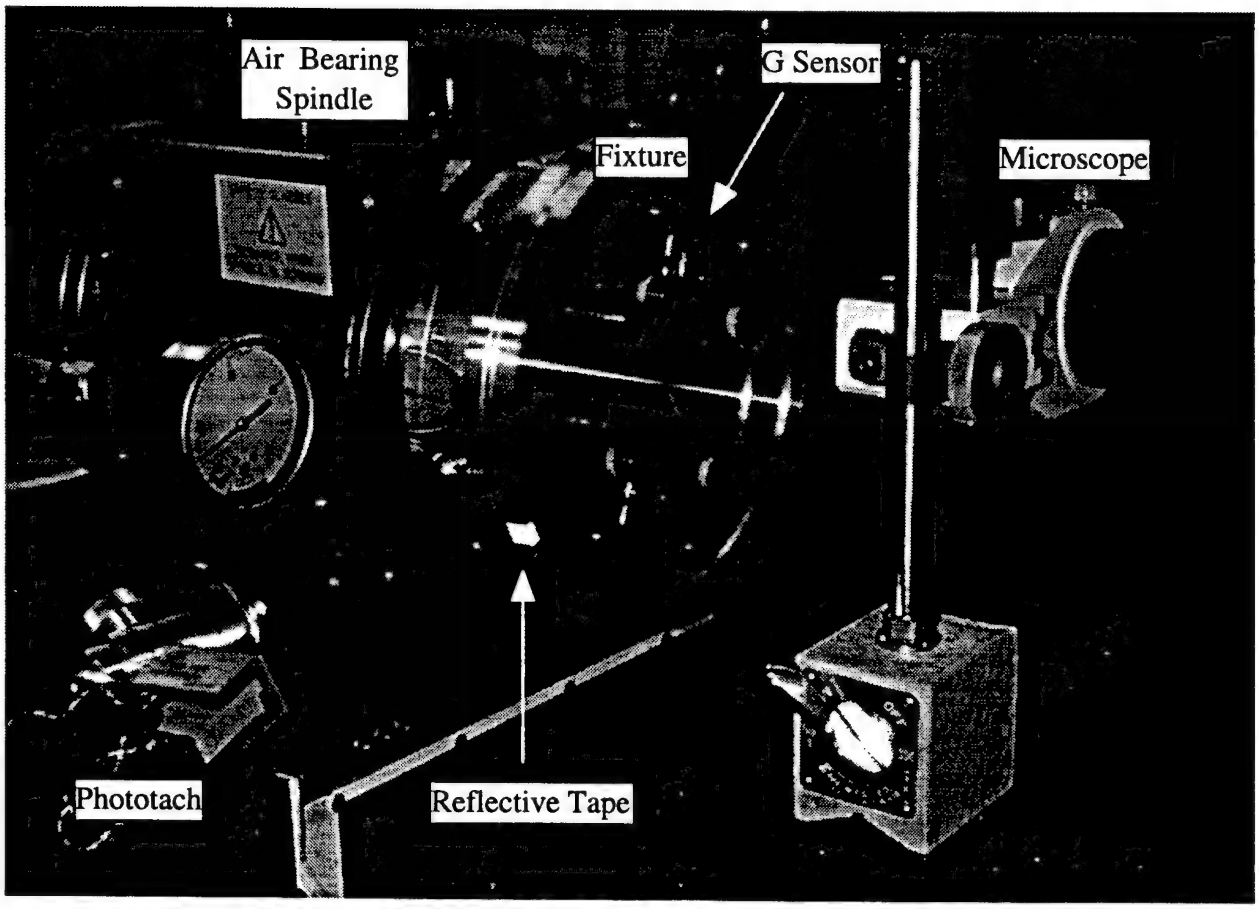

Figure 2: Setup on Precitech diamond turning machine. First round of testing. Strobe and camera are not shown in this photo for clarity.

The video zoom microscope provided magnifications ranging from 40X to 140X on the 13" video monitor. This range of magnifications seemed ideal for these measurements. The camera used to record the testing was a Pulnix TM 9701 Progressive Scan camera. This camera was chosen because it captures the image with a high resolution non-interlaced CCD array, but outputs an interlaced signal compatible with NTSC devices. The ability of the camera to acquire images in a noninterlaced mode prevents the image of a moving object to appear smeared because the object has moved between the scanning of the odd and even video lines.

The TM 9701 has the ability to capture images via an external trigger. This capability was not utilized in this experiment, but would allow the strobe light to be eliminated from the setup. The ability for the shuttering to be independent of the lighting of the sample might be advantageous in future experiments. Proper lighting of the sample seemed to be the most difficult obstacle in all of the experiments.

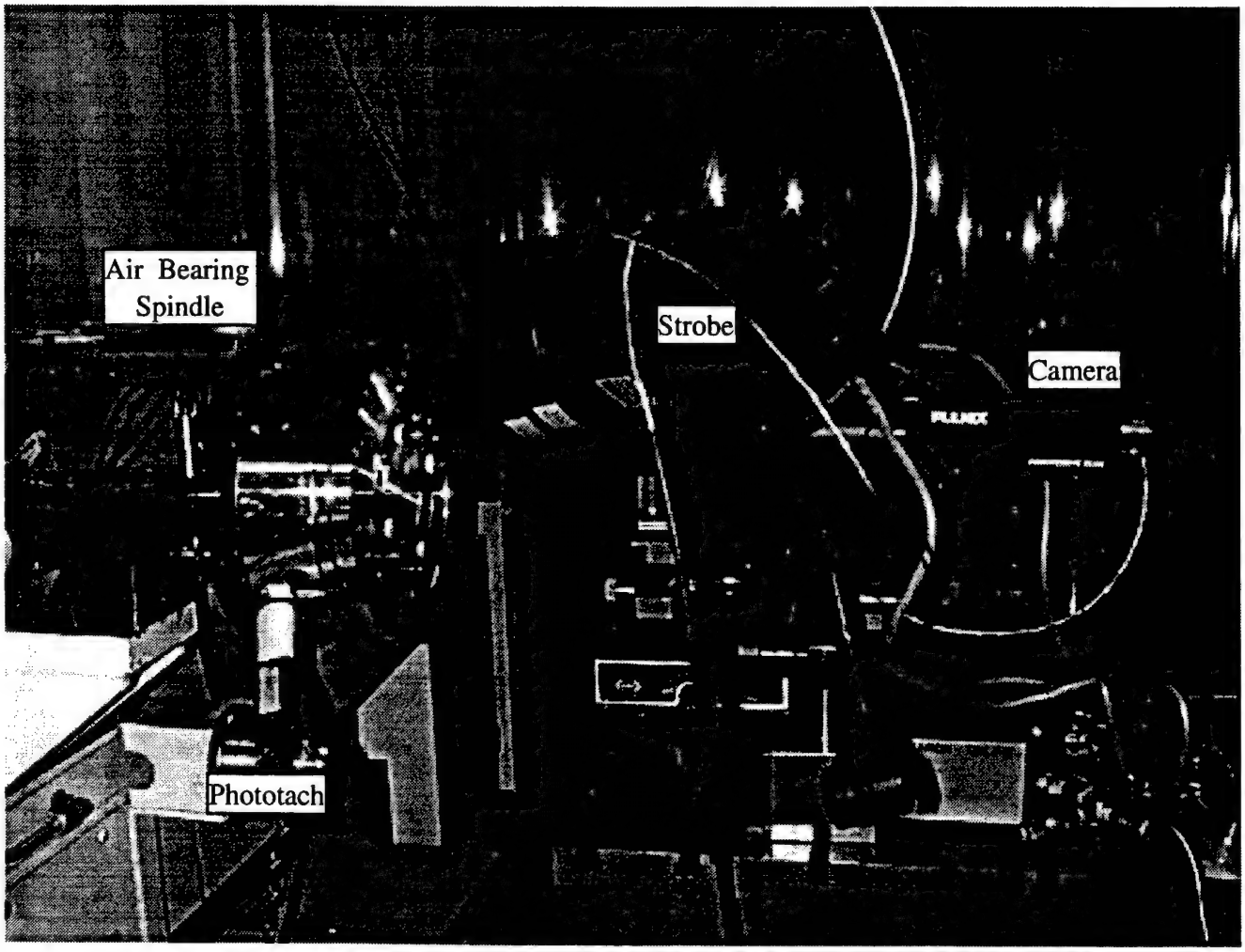

Figure 3: Nanoform 600 test setup during the second round of spin tests.

Lighting problems were attributed to the high reflectivity of the silicon samples. Due to the highly reflective silicon surfaces, the light from the strobe seemed to reflect past the microscope. The sensors were examined with the video microscope prior to testing. During this examination they were lit with a fiber light placed parallel to the microscope tube and very close to the microscope. This setup provided very good lighting, however during testing it was not possible to align the larger strobe in the same manner as the fiber light. To improve lighting, a second strobe was added. Also, it was noticed that the Sony video printer seemed to provide some amplification of the image signal, so the signal was passed through the video printer before it went to the VCR.

The data for the experiment was recorded on a JVC HR-S5400U Super VHS VCR. This VCR was chosen due to the enhanced resolution of the Super VHS video and the still picture frame-by-frame playback capability. We had the capability to grab images of the sensors with a frame grabber during testing, however this would have significantly increased the duration of testing due to the time required to save the graphics files. The frame grabber was often used to freeze images of the sensor during testing if critical measurements were necessary, and during these tests the frame grabber was mostly used as an item of convenience.

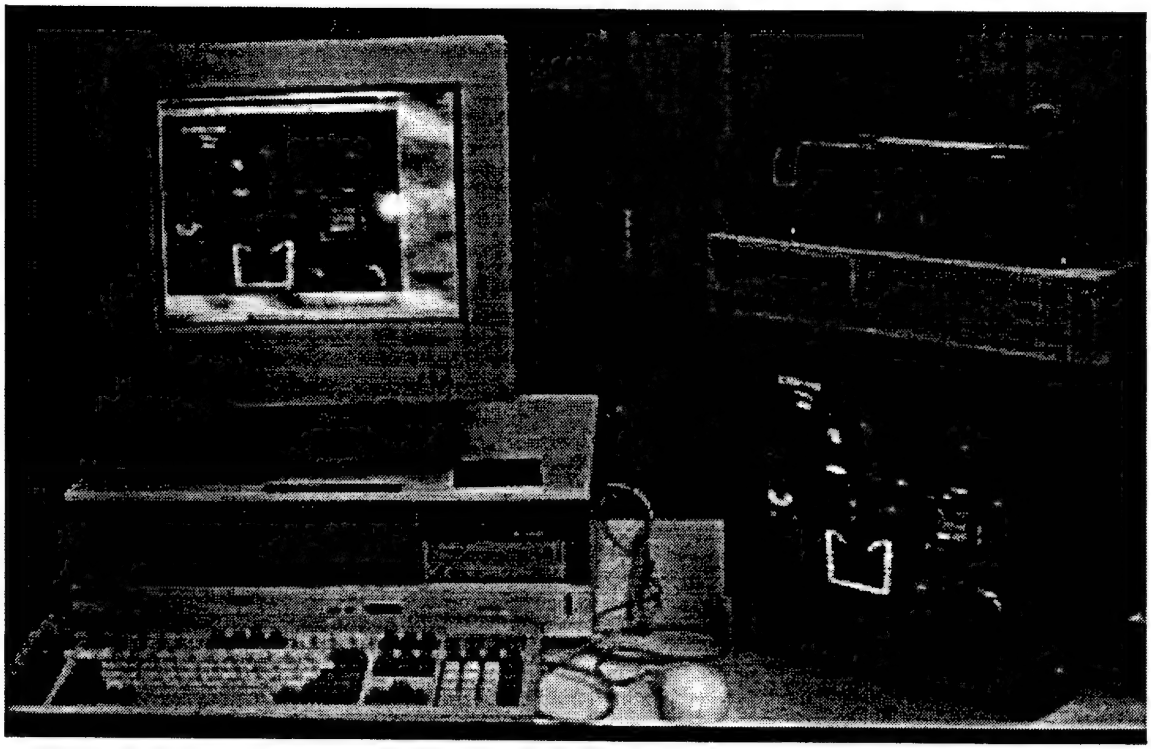

Figure 4: VCR, video printer, monitor and frame grabber setup. Image from camera and frame grabber. (Image is from video tape of the first round of testing.)

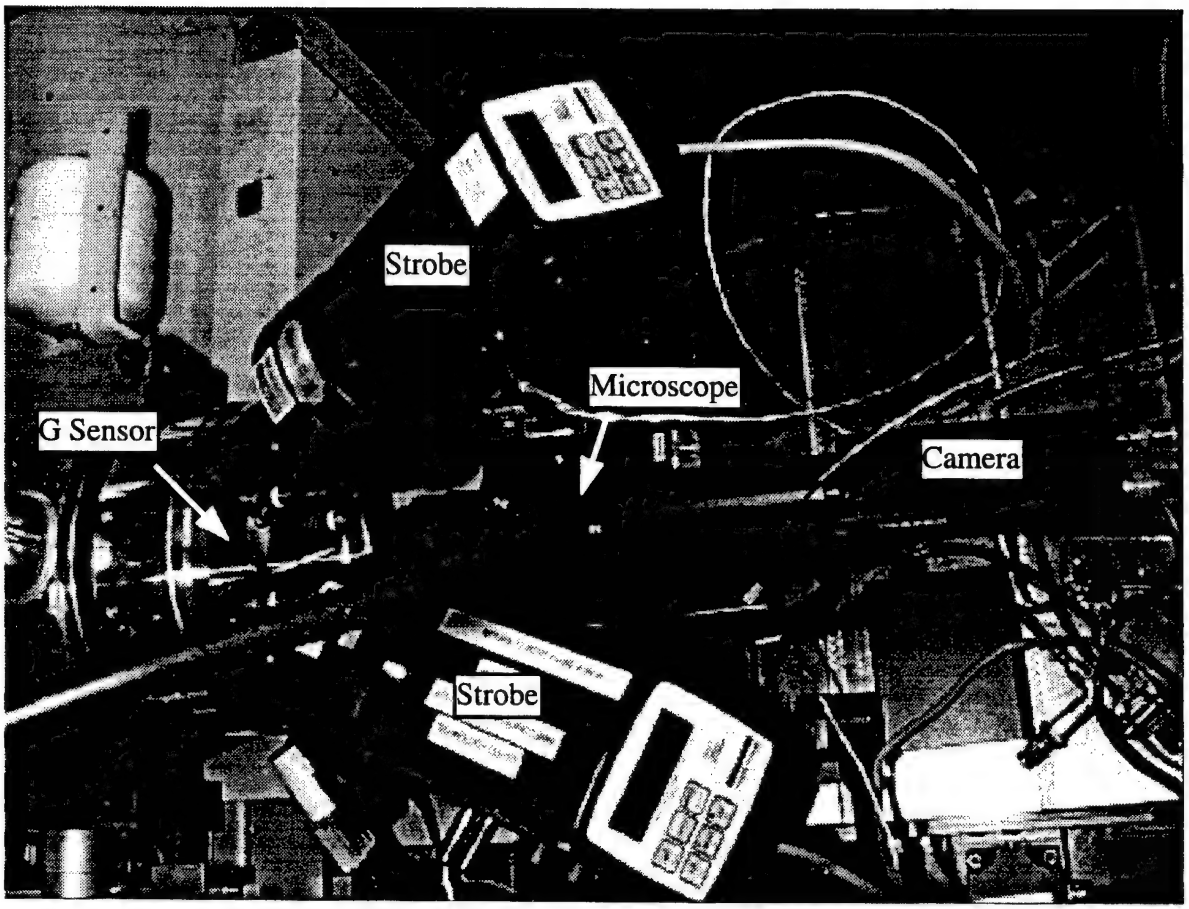

Figure 5: Top view of test setup for second round of testing.

Test Procedure

During the test sequence, the sensor to be tested was mounted in the test fixture with the optical bench clamps. The sensor was video taped at rest in order to document its condition prior to testing. The sensors in the first round of testing were spun up in 10g increments until latching occurred or until a maximum of 60 g's (1080 RPM) acceleration was reached. In the second round of testing, the sensors were spun up in 5g increments to obtain a more accurate value of the latching acceleration. These were spun up to a maximum of 120 g's. Once the latching g load was reached, the sensors were spun down in 10 g increments to ensure that the latch would not release once the load was released. Finally, the "at rest" condition of the sensor after the test was recorded on video tape. During testing, the tape counter position was recorded with the g load and sensor identification. Several of the sensors were manually "unlatched" and tested again in order to obtain some idea of the repeatability of the latching forces.

Some of the sensors were tested with a scheme intended to simulate a sudden spin up. The g load was increased in 5 g increments, however the load was returned to zero between each loading. Therefore each load started from zero and rapidly ramped up to the desired load in approximately 3 seconds. It was observed that one of the dominating factors in the load required for latching was the friction between the latch and the plunger. The sudden loading test was used to determine the effect that latching velocity had on the load required to latch the sensor. It was hypothesized that rapidly spinning up the sensors might cause them to latch at a lower acceleration due to the phenomena that the coefficient sliding friction is less than objects at rest. Rapidly spinning up the sensors from 0 g's to the test level did not appear to change the latching load level.

Observations

Several observations were noted during the sensor testing. Two strobes were required to provide sufficient lighting of the sample. Even with two strobes, some amplification of the signal with the video printer helped improve the clarity of the image. Some of the sensors were manually "unlatched" so that they could be tested again. It appeared that manipulating the latches could very significantly impact the g load required for latching. Zooming the microscope out to view the entire test structure and check the condition of the springs was helpful in determining the condition of the sensor and verifying the design. Recording the start and stop times on the tape for each g level helps to locate individual measurements during post test analysis of the video tape. Finally, the sudden up sudden down load tests did not appear to have any influence on the latching load or the ability of the sensor to remain latched.

Future Recommendations

Improvements in sensor lighting would probably make the most difference in the quality of the test. Synchronization of the camera with sensor rotation would allow the lighting to be independent of "shuttering". The change to camera shuttering might complicate the setup, but would likely improve the quality of the image and not subject the test operator to hours spent in a dim light room with a flashing light. The TTL signal from the phototach can be used to determine the actual RPM that the spindle is operating. This actual RPM value would be a more accurate way to calculate the g load. Also, slight changes in the RPM caused the image to drift of appear to bounce during testing. The RPM or frequency should be sampled more than once per revolution to improve synchronization. Finally, in the second round of testing speeds in excess of 2,000 RPM were required to latch some of the sensors. In the future, if these loads are required the larger radius on the fixture should be used for safety concerns.

Figure 6: Howard Last unlatches g load sensors between testing.

CHARACTERIZATION OF MEMS DEVICES UNDER THE CTIP GRANT TO MCNC

FINAL REPORT

Reporting Period August 1997 - June 1998

Contract: C97-5113-822

Prepared for:

Dr. Howard R. Last
Naval Surface Weapon Center - Indian Head Division
Code 420C5, Bldg 301
101 Strauss Ave.
Indian Head, MD 20640-5035
(301) 743-6726

For Questions Please Contact:

Edward V. White
Manager, Smart Structures and Systems
The Boeing Company
Mailcode S1021310
P.O. Box 516
St. Louis, MO 63166-0516
(314) 232-1479
edward.v.white@boeing.com

FINAL REPORT FOR CHARACTERIZATION OF NSWC MEMS DEVICES UNDER THE CTIP GRANT TO MCNC

Table of Contents

FINAL REPORT FOR CHARACTERIZATION OF NSWC MEMS DEVICES UNDER THE CTIP GRANT TO MCNC

List of Figures

List of Tables

FINAL REPORT FOR CHARACTERIZATION OF NSWC MEMS DEVICES UNDER THE CTIP GRANT TO MCNC

Introduction

This report documents a series of tests to characterize Safe and Arm (S&A) Micro-ElectroMechanical System (MEMS) devices and components. This work was performed for the Naval Surface Warfare Center (NSWC) under contract to MCNC under the Commercial Technology Insertion Program (CTIP). All devices tested were provided by NSWC.

The testing was divided into two tasks. The objective of Task 1 was to measure the force-displacement characteristics of selected MEMS S&A devices. This testing made use of the MEMS device force measurement station developed under the DARPA Active Materials for Photonics Systems (AMPS) program, contract DAAH04-95-C-0007.

The objective of Task 2 of this effort was determination of the dynamic response characteristics of several MEMS S&A devices.

Testing under both tasks were performed in two groups, the first in September of 1997 and the second in June 1998.

Task 1—Force - Displacement Testing

Task 1 is the precision force and displacement testing of suspended spring structures (g-sensor, slider/barrier and actuator slider structures) supplied by NSWC. Mounted MEMS devices were tested in two groups on the existing Active Material for Photonic Systems (AMPS) program MEMS characterization station. The measurement station is described fully in Appendix A, "Direct Measurement of Force and Displacement of LIGA Micro Springs and Actuators" by John M. Haake (The Boeing Company) and Robert L. Wood and Vijayakumar R. Duhler (MCNC).

Figure 1 illustrates the test set-up. Figure 2 illustrates the force probe calibration. The force probe calibration constant (stiffness) should approximate the following relationship for bending of a cantilever beam.

$$Stiffness = \frac{Force}{\Delta X} = \frac{3E(\pi D^4 / 64)}{L^3}$$

Where: E = Young's Modulus (typically 73 GPa for silica optical fiber)
D = Diameter of optical fiber (diameter of cladding)
L = Length of fiberoptic cantilever

Figure 1. MEMS Force and Displacement Measurement Station

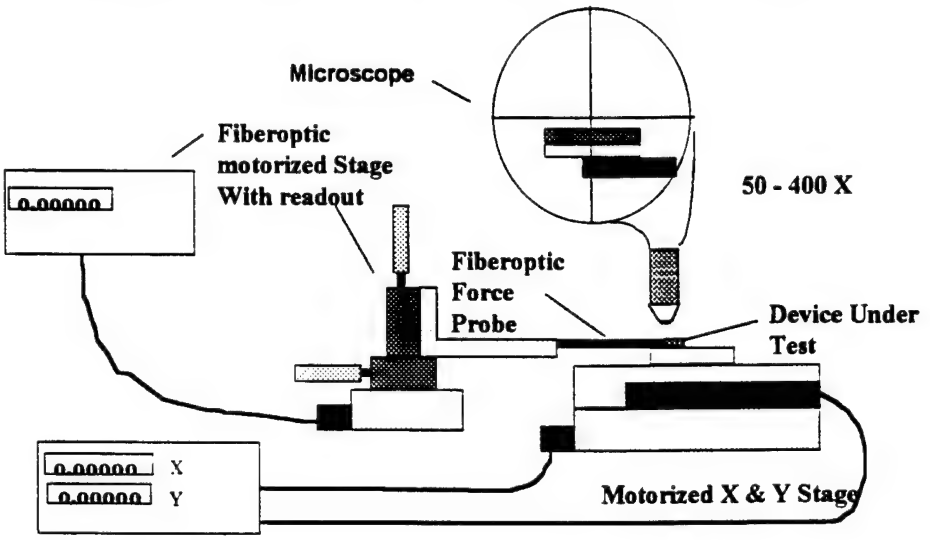

Figure 2. Calibration of Fiberoptic Force Measurement Probe

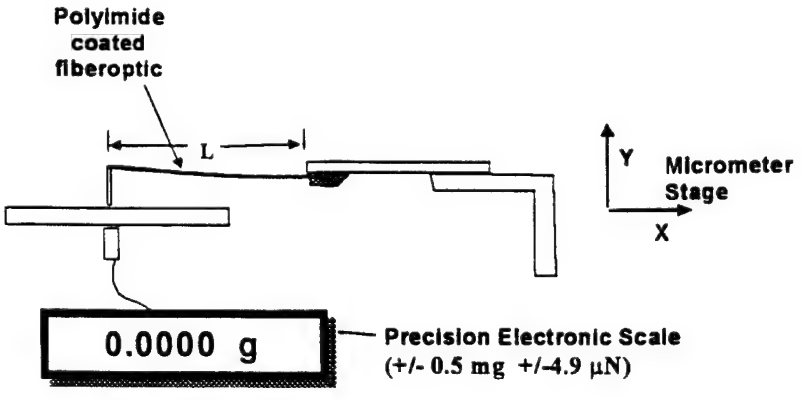

Force Probe Calibration Procedure – The calibration of the force probe is a simple procedure using a precision electronic scale to measure force and a micrometer stage to measure displacement. The objective is to determine the calibration constant of the force probe (equivalent to its stiffness). The equipment used was:

Metler AE163 Precision Electronic Scale (MDC property number 118001)
Oriel Micrometer Stage (MDC property number 16614)

The procedure follows:

1. Align the probe with horizontal.
2. Zero the electronic scale.
3. Using the micrometer stage, align the force probe so it is just touching the cover slide on the electronic scale.
4. Note the micrometer reading as the zero point.
5. Zero the electronic scale.
6. For the first 10 mils of measurement: move the micrometer stage down 1 mil per step and record the scale reading at each 1 mil increment.
7. For the remainder of the measurements: move the micrometer stage down 2 mils per step and record the scale reading at each 2 mil increment.

Raw data for calibration of the probe designated 15.4-1 is shown in appendix B. Raw measurements in milligrams and mils are converted to milliNewtons (mN) and millimeters (mm). Each of three calibration trials is shown. Data was converted to units of mN/mm and each of the three trials was fitted to a straight line using unweighted least squares. An example plot for Trial 1 with a straight line fit is shown in Figure 3. Complete calibration results are summarized in Table 1.

Figure 3. Probe 15.4-1 (200/240 Fiber) Calibration, Trial 1

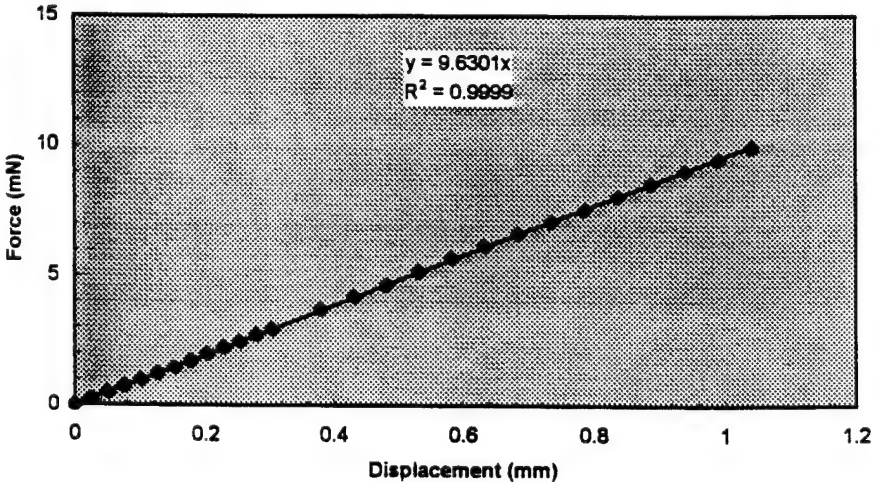

	Calibration Constant (mN/mm)	Least squares correlation constant
Calibration Trial 1 *	9.63	.9999
Calibration Trial 2 *	9.69	.9997
Calibration Trial 3 *	9.70	.9997
Average of 3 trials	9.68	N/A
Theoretical	9.766	N/A

* Note that one outlying point was dropped from the data set of each trial that did not lie on the respective lines. This made no difference in the average calibration constant.

TABLE I. Force Probe Calibration Summary for Probe 15.4-1

Note that the measured calibration constant is less than 1% different from the theoretical value. The measured constant will be used in the force – displacement measurements in this report, but if measured calibration data are not available, the theoretical calibration value can be used with little error introduced. Note that in the theoretical calculation length of the probe appears raised to the third power. Care should be taken in measurement of this length.

Force – Displacement Measurement – The objective of the force – displacement measurements is to characterize the stiffness of the MEMS device or component. Measurements were made using the following equipment (illustrated in Figure 1):

Reichert McBain (Nikon) Microscope (MDC property number 111962)
Force Probe 15.4-1
Metronics Quadra-Chek II Displacement Readout
(MDC property numbers 111962-008 and 111962-009)
Aerotech Inc Stage and Readout (MDC property number 688926)

The procedure is as follows:

1. Align the horizontal cross-hair in the eyepiece with the horizontal travel of the microscope stage.

2. Install the force probe so that the anvil is orthogonal to the microscope stage.

3. Position the force probe so that it travels along the horizontal cross-hair as it is translated by the slew controller.

4. Attach the device to be tested firmly to the microscope stage.

5. Adjust the device so that the beam to be measured travels along the horizontal cross-hair as the stage is translated.

6. Pick a mark on the beam, set the cross-hairs on that mark and set the microscope micrometer readout to zero.

7. Translate the beam the desired amount with the microscope micrometer.

8. Using the slew controller, bring the anvil into contact with the beam without moving it and zero the slew counter.

9. Slide the beam using the force probe until the mark is back on the cross-hairs and stop. Record the displayed slew value.

10. Back the force probe away until it is out of contact with the beam.

11. Repeat steps 6 thru 10 as many times as desired at different displacements.

The raw data from the force - displacement testing must be converted to engineering units of displacement. The base movement must be subtracted from tip movement of the force probe to give the displacement of the tip relative to the base.

Two sets of force – displacement testing were conducted as described below. The primary information to be determined from displacement - force testing is the measurement of the spring constants (stiffness) of the devices.

Test Set 1 (September 1997):

During September 1997 Displacement - Force testing was performed on the following devices: 2B, 2C, 2D, 2E and 2F. The computed stiffness data (averaged over two trials on each device) are summarized in Table II.

Device	Number of Trials	Averaged Stiffness (milliNewtons/micron)
2B	2	0.00864
2C	2	0.0192
2D	2	0.0173
2E	1	0.0192
2F	2	0.0154

Table II Averaged Stiffness Data from Test Set 1

The measured data are plotted in Figures 4 through 8.

Figure 4 - Device 2B Displacement - Force Testing

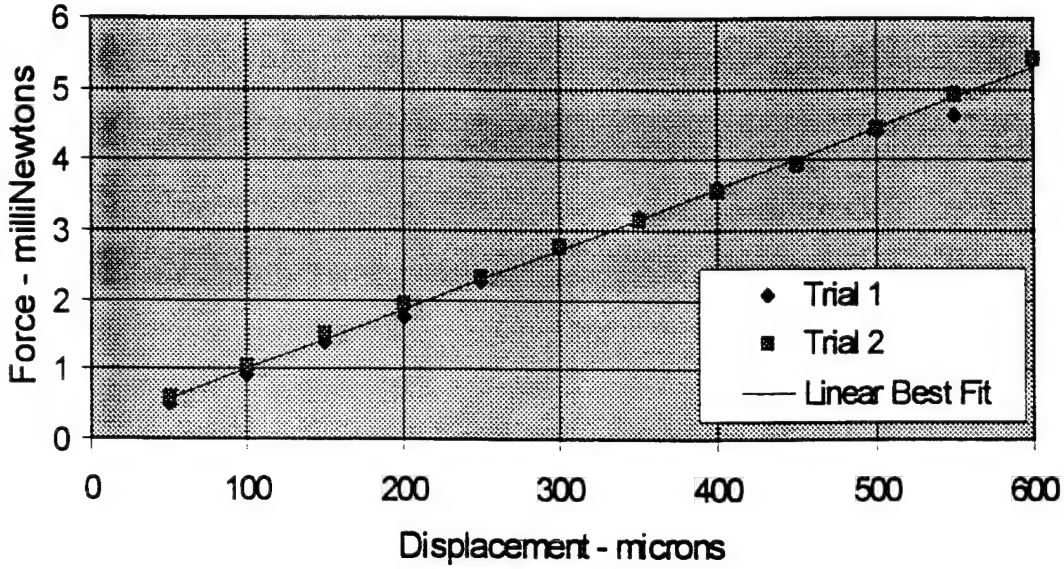

Figure 5 - Device 2C Displacement - Force Testing

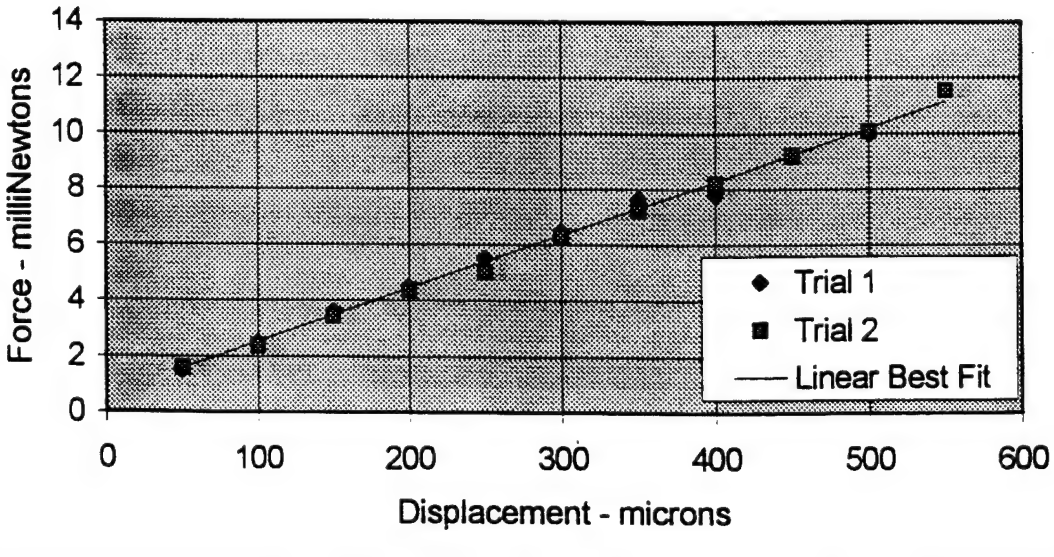

Figure 6 - Device 2D Displacement - Force Testing

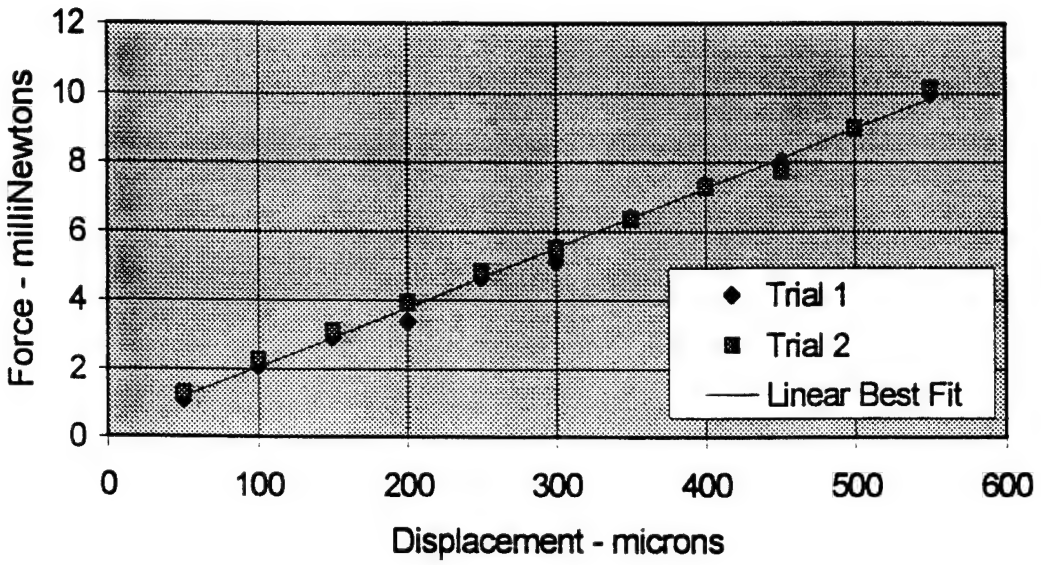

Figure 7 - Device 2E Displacement - Force Testing

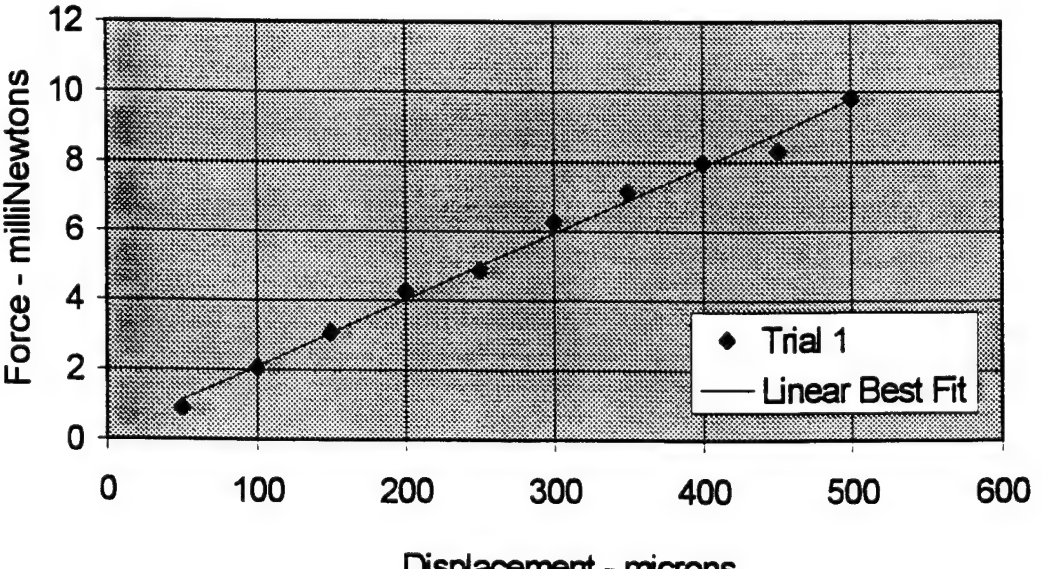

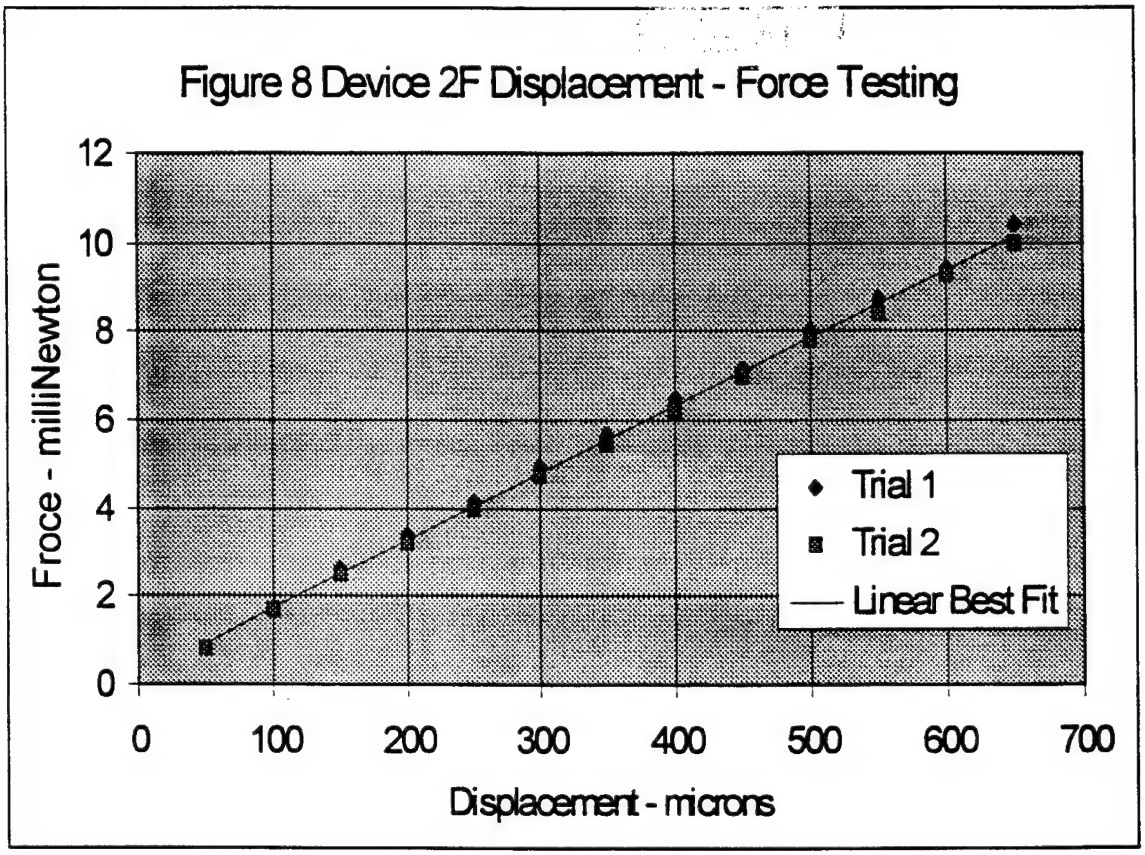
Figure 8 Device 2F Displacement - Force Testing
Froce - milliNewton
12
10
8
6
4
2
0
0
100
200
300
400
500
600
700
Displacement - microns
Trial 1
Trial 2
Linear Best Fit

Test Set 2 (June 1998):

During the second set of testing Force Probe 15.4-1 described above was used to remeasure forces on the device designated 2E. Two trials were conducted. Figure 9 illustrates trial 1of this test set. As shown, the measured displacement vs. load was fit to a straight line yielding a slope (stiffness) of 0.0173 mN/micron with a correlation coefficient of 0.9986. Showing very good repeatability, the second trial yielded a stiffness of 0.0172 mN/micron with a correlation coefficient of 0.9988. Stiffness measurements during the first set of testing measured 0.0192 mN/micron for this device. The reason for this difference is most likely due to the fact that one of the spring legs on the 2E device was noticed to be bent during the second series of testing. This most likely resulted in the lower measured stiffness during the second test series.

Figure 9 - CTIP Round 2, Part 2E Test #1

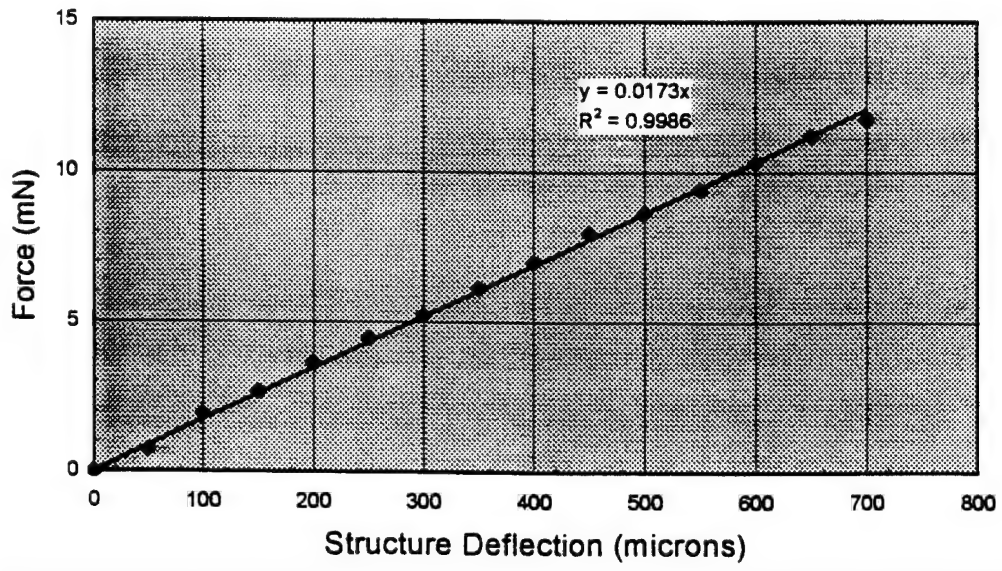

Displacement - force measurements were made on two other devices designated 2TC-1#4 and 2C. Device 2TC-1#4 encountered a stop at approximately 225 microns so measurements were made only up to 200 microns. These data are shown in Figure 10. Data for the three trials shows the measurement to be fairly repeatable. The average slope (stiffness) of the three trials is 0.0367 mN/micron. The linear regression correlation coefficient of 0.99938 indicates that the device spring response is quite linear. Trial 2 showed the largest deviations from a linear best fit (up to 3.34%) with the lowest correlation coefficient of 0.9983. Removing Trial 2 from the data set gave a stiffness of 0.0365 mN/micron with a correlation coefficient of 0.9997 and the largest deviation from linear of 1.41%. It is not known why trials 1 and 3 matched so well and trial 2 differed by 1-4%. This is indicative that the overall

accuracy of these measurements should not be presumed to be much better than ±5% unless a large amount of measurements are conducted.

Figure 10 Displacement - Force for Specimen 2TC-1#4

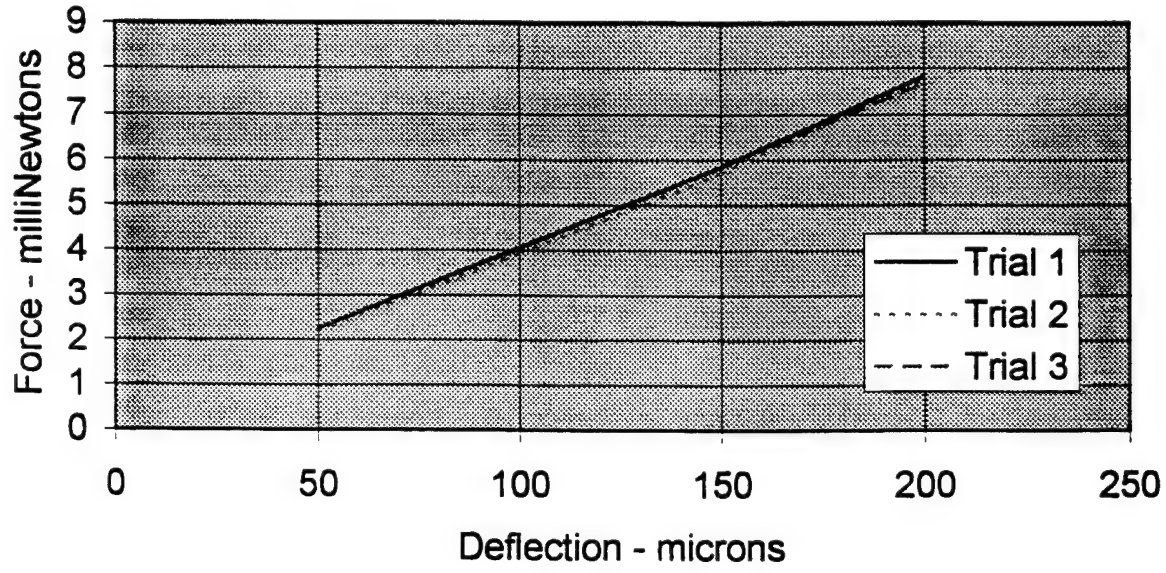

Displacement - force measurements for Device 2C are plotted in Figure 11. This device showed some nonlinear response. The stiffness of the device appeared to

Figure 11 - Displacement - Force for Device 2C

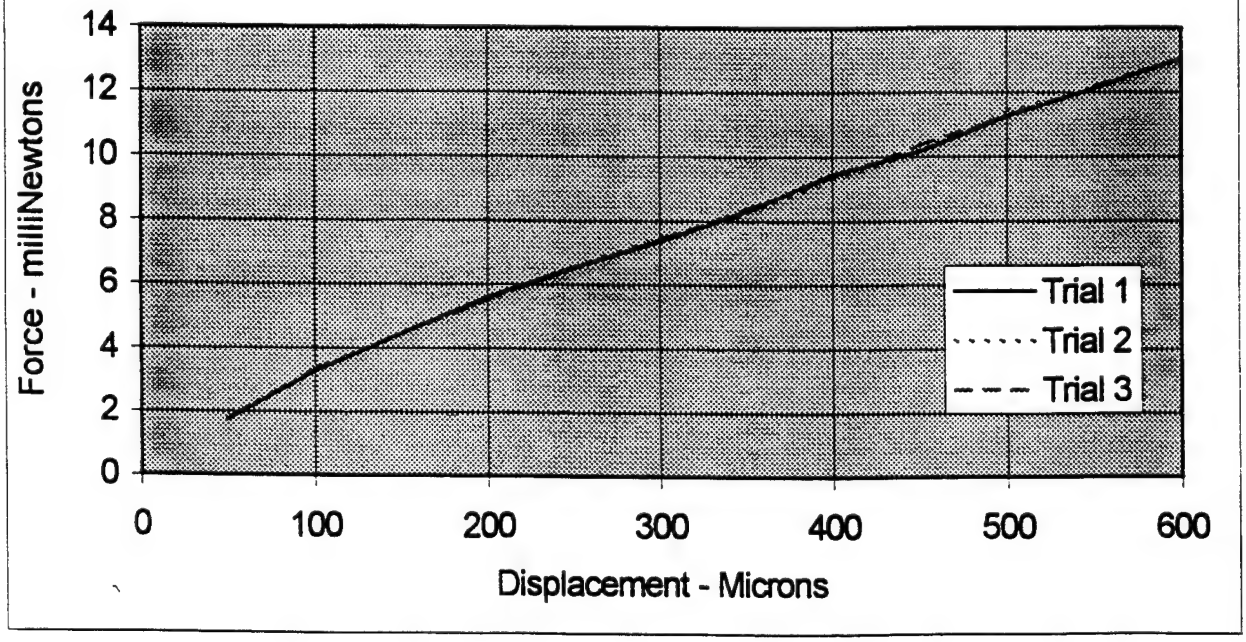

decrease slightly as displacement increased. Although the plot seems to show the stiffness stabilizing above about 100 microns of displacement, there was still some nonlinearity present. Using only the data for 100 microns and above, the average stiffness of the three trials was 0.0193 mN/micron. The linear regression correlation coefficient was 0.9992. Although this is a good correlation coefficient, the deviation from linear was always largest (4-6% at 100 microns) at the lowest displacements indicating the nonlinearity is not due to a measurement error at 50 or even 100 microns. Also, the technician noted that the motion of the device was not smooth, particularly around 300-350 microns. The first test series measured a stiffness of 0.0207 mN/micron for this device.

Task 2—Resonant Frequency Characterization

The objective of the resonant frequency vibration testing was to characterize out-of-plane vibration modes of g-sensors, suspended spring structures, and latching devices. Where possible, additional information such as a qualitative description of the resonant mode shape and an estimate of the mode quality factor / damping were recorded.

Mounted NSWC devices were characterized on a self-constructed resonant frequency characterization station. Amplitude and frequency of the MEMS devices were characterized with a frequency resolution of 1 Hz and an amplitude displacement resolution of 5 microns. In general the characterization station, illustrated in Figures 12 and 14, consisted of a piezoelectric vibration exciter to apply controlled vibration to the device and a non-contacting laser vibrometer to measure the resonant response of the device elements.

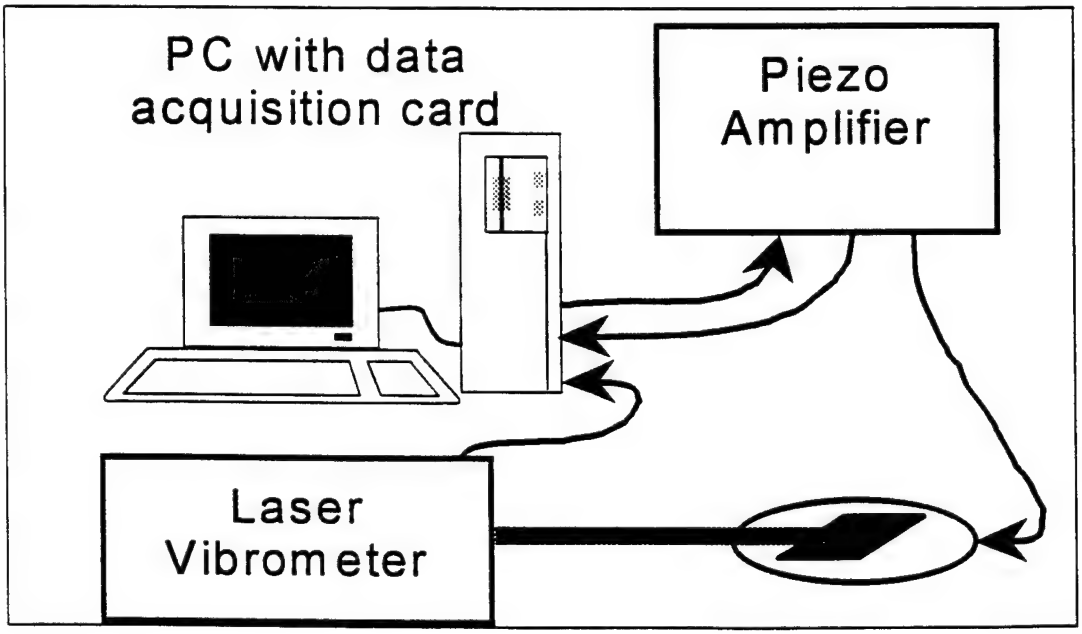

Figure 12 Test Set 1 Resonance Measurement Setup

The first group of devices was characterized using a two method process. First, a PC with a plug-in data acquisition card and LabVIEW software is used to generate a band limited, white noise random signal, which drives the Piezo-amplifier, which drives the piezo-actuator (See Figure 12). Simultaneously, the PC samples both the piezo-actuator voltage and the laser vibrometer output. The acquired data are processed using LabVIEW's Power Spectrum function. The resultant data are plotted and used to determine the frequency of the resonant vibration modes of the

device. An example of the data is shown in Figure 13. Both drive and response signal spectra are plotted.

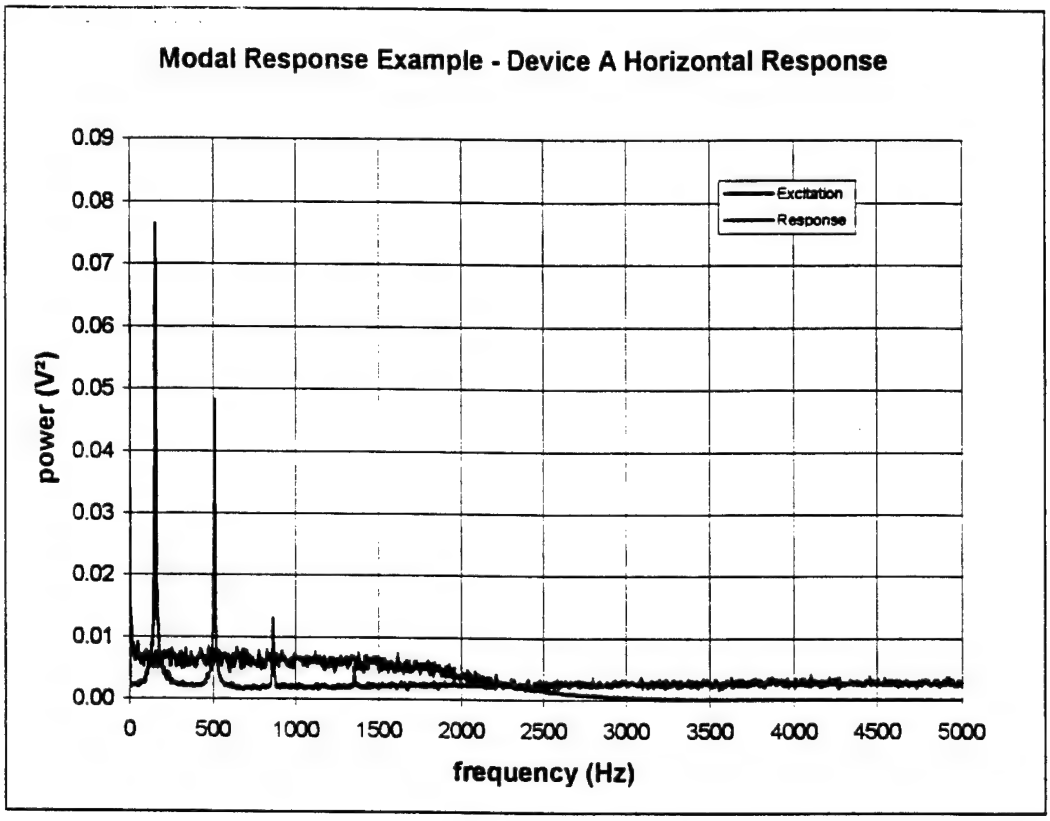

Figure 13 Modal Response Example

In Test Set 2 the test setup illustrated in Figure 14 was used to measure the resonant frequencies and amplitudes. A sine wave signal generator drives the Piezo-amplifier, which drives the piezo-actuator. The '÷20' output is also monitored on the scope to verify the drive signal quality. The frequencies and amplitudes are measured at several locations on the device by slowly sweeping the input frequency and observing amplitude maximums on the oscilloscope. The base motion is also measured so that damping can be estimated. The second group of devices was tested using only this second test method because the software used to generate the random signal was inadvertently lost after the first test group was completed and could not be recreated in the time available.

The relative advantages of the first method are that all modes are excited simultaneously. Frequencies are easily identified, but little other meaningful information can be reliably obtained. The second method requires manual tuning of the excitation frequency to identify the resonances and hence requires significantly more time. The advantage of the second method is that it facilitates estimation of the damping of each identified mode and provides a more meaningful (qualitative)

characterization of the device dynamics. For this type of testing it is recommended that method 2 be used in the future unless the device response to a random vibration environment is specifically desired. Test methods are available to use random data to extract the full set of resonance information (frequency, damping and mode shape) but such methods are beyond the reasonable capabilities of the current equipment.

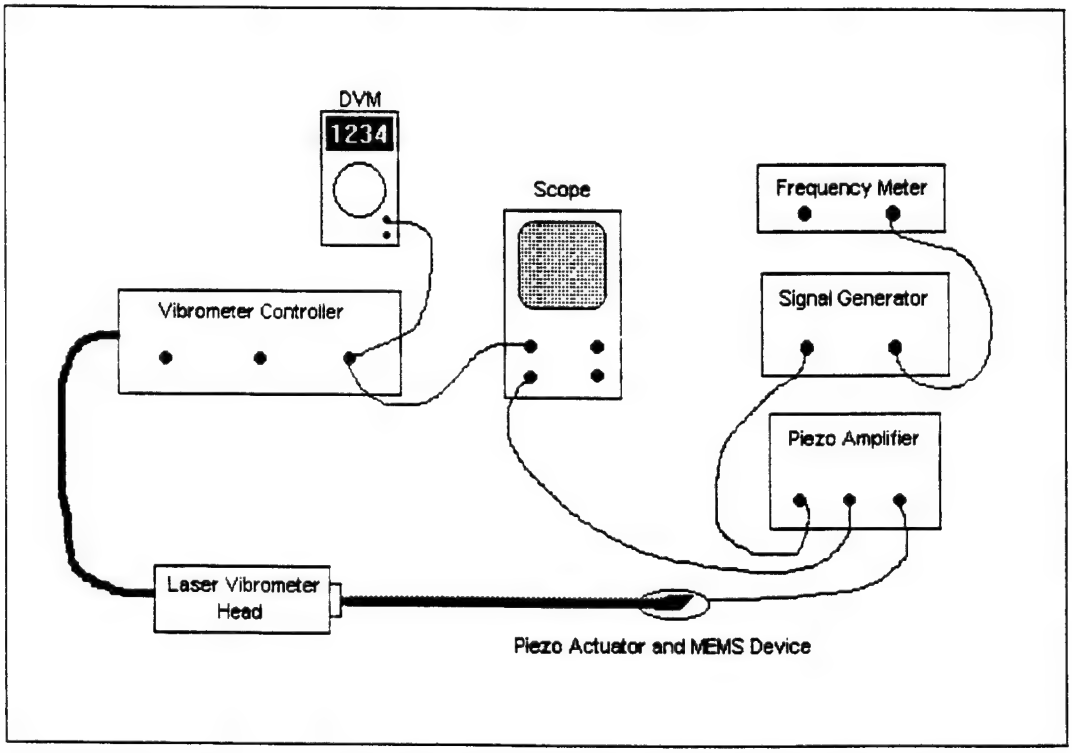

Figure 14 Test Set 2 Resonance Measurement Setup

The following equipment was used for method 1 of the Resonant Frequency Characterization:

Polytec Laser Vibrometer Model OFV 2100 with Sensor Head Model OFV 300
AVC Instrumentation Power Amplifier Model 790 Series
Physik Instrumente Piezo Actuator Model P-286.40
PC with Labview software and National Instruments A/D and D/A board

The following equipment was used for method 2 of the Resonant Frequency Characterization:

Polytec Laser Vibrometer Model OFV 2100 with Sensor Head Model OFV 300
AVC Instrumentation Power Amplifier Model 790 Series
Physik Instrumente Piezo Actuator Model P-286.40
Hewlett-Packard Frequency Counter Model 5334B
Tektronix Oscilloscope Model 7603

Fluke Digital Multimeter Model 79

The piezo-actuator was isolation mounted (with foam tape) on a two-axis translation stage. The MEMS device was hard mounted to a ceramic carrier, which was hard mounted to the piezo-actuator using double-sided tape. A 45-degree mirror was mounted on a separate stage directly above the device to turn the laser beam from horizontal to vertical. (Mirror not shown in figures).

Like the displacement -force testing, the resonant frequency testing was done in two groups. The piezo actuator used had its lowest self resonance at a frequency of about 1600 to 2000 Hz, depending on the mass of the device under test. All data above this actuator resonant frequency was discarded.

Test Set 1 (September 1997):

A large amount of resonance testing data was obtained on the devices 2B, 2C, 2D, 2E and 2F. An attempt was made to extract damping information from this data. However, the noise in the measurements does not permit extracting reliable damping estimates. Resonant Frequencies are readily identified and have been summarized in Table III. All frequencies are given in Hertz.

Device	Direction of Test	Frequency 1	Frequency 2	Frequency 3
A	Horizontal	156	513	864
A	Vertical	146		
B	Horizontal	264	933	
B	Vertical	537	947	
C	Horizontal	293	938	
C	Vertical	557	957	
D	Horizontal	No Resonances Detected		
D	Vertical	254	889	
E	Horizontal	181	913	
E	Vertical	186	601	
F	Horizontal	132	815	
F	Vertical	161	600	957

Horizontal refers to in the plane of the device
Vertical is out of the plane of the device

Table III - Summary of Test Set 1 Device Resonant Frequencies

Test Set 2 (June 1998):

The highest priority for resonance testing in the Group 2 devices was for the two Phase IV devices. Unfortunately the Phase IV device numbers A9 and 435 (Design 1) were both tested but were found to be "locked" to the degree that we were unable to excite any resonances below 2000 Hz. The term "locked" means the devices had elements contacting the main sliding element, which effectively damped any vibration modes the devices would have had. For the devices that could be successfully tested in the time available, the results of the resonant frequency testing are summarized in Table IV.

Device	Mode Frequency - Hz	Mode Description	Estimated Damping Ratio	Estimated Q
2C	561.5	Rocking	0.0059	85
2C	962.7	Plunge	0.0010	481
3(A)-175	678	Plunge	0.0039	128
3(A)-175	1246	Rocking	0.0024	208
3(C-1)-175	519	unknown	0.0048	104
3(C-1)-175	973	unknown		
3(D-1)-175	696	unknown	0.0357	14
3(C-3)-175	537	Plunge	0.0093	54
3(C-3)-175	940	unknown	0.0059	85
3(C-3)-175	1255	Rocking	0.0064	78

TABLE IV - Test Set 2 Resonant Frequency Testing Results Summary

Interpretation of Results - Frequency - Although a highly accurate frequency meter was used to measure the frequency, the measurement is dependant upon manually tuning the exciter frequency to maximize the response. This process can be difficult, particularly if the mode is lightly damped as many of the modes were found to be. It was also found that excessive input amplitude resulted in grossly nonlinear response. It is suspected that at resonance the sprung component may respond so much that it impacts the base of the device. This nonlinear response is characterized by difficulty in tuning to the resonance, which seems to change frequency, and by the appearance of non-sinusoidal response or response at multiple frequencies. In all cases in the Group 2 testing, the amplitude of the input was reduced as needed to produce a clean sinusoidal response at the driving frequency. The difficulty of this

tuning process indicates that the accuracy of the frequency measurements should be considered as no better than +/- 2%.

Further, the piezoelectric exciter was found to have a resonance of its own at approximately 1500 Hz (unloaded). When loaded with the device under test, this resonance was reduced to the range of 1418-1500 Hz. Thus any resonances observed in or near this frequency range are most likely due to the test method and are not a true resonance of the device.

Interpretation of Results - Mode Description - In some cases it was possible to compare the relative amplitude response of two or more modes and qualitatively characterize the mode as either predominately a vertical translation of the sprung component, termed plunge, or as a rocking of the component. This characterization was not possible with all the devices.

Interpretation of Results - Damping/Q - Where possible, an attempt was made to estimate the damping inherent in the vibration mode. Two methods were used to estimate this damping. Measurements were made both of the response of the component under test and of a nearby point on the base of the device. The Q or Quality Factor of the resonance can then be estimated from the ratio of the response of the component at resonance to the motion of the base at the same frequency. Alternatively, once a resonance was found, we attempted to tune to the half power points on either side of the resonance and record the frequency. The Q of the resonance can then be calculated from:

$$Q = \frac{f}{\Delta f}$$

Where: f = frequency at resonance

Δf = difference between the frequencies at the half power points

Q is directly related to damping as:

$$\zeta = \frac{1}{2Q}$$

Where: ζ = ratio of damping to critical damping

The maximum displacement response in any mode to any vibration excitation can be estimated as follows:

For sinusoidal vibration:

$$\delta = \frac{\ddot{Z}Qg}{(2\pi f)^2}$$

Where: δ = maximum displacement (units consistent with g)
$\ddot{Z}$ = sinusoidal vibration acceleration amplitude (g's - peak)
g = acceleration of gravity

For random vibration:

$$\delta = \frac{3g}{(2\pi f)^2}\left(\sqrt{\frac{\pi}{2}SfQ}\right)$$

Where: δ = maximum displacement (3σ, units consistent with g)
S = Power Spectral Density of input vibration at f (G^2/Hz)

APPENDIX A

Direct Measurement of Force and Displacement of LIGA Micro Springs and Actuators

John M. Haake, Robert L. Wood, Vijayakumar R. Duhler, Howard R. Last

FINAL REPORT FOR CHARACTERIZATION OF NSWC MEMS DEVICES UNDER THE CTIP GRANT TO MCNC

Direct Measurement of Force and Displacement of LIGA Micro Springs and Actuators

[a] John M. Haake, [b]Robert L. Wood, [b]Vijayakumar R. Duhler, [c]Howard R. Last

a) The Boeing Company, PO Box 516, St. Louis, MO 63166
b) MCNC, 3021 Cornwallis Rd., PO Box 12889, Research Triangle Park, NC 27709
c) Naval Surface Warfare Center,. Indian Head MD 20640-5035

ABSTRACT

We describe and demonstrate an inexpensive and accurate means of measuring force and displacement of LIGA micro springs and actuators. This method has a large dynamic range from 10 micro-Newtons to 100's milli-Newtons with accuracies of a few percent. The force and measurement station is completely described and a means for automation is discussed.

Keywords: Force measurement, Displacement, Micro-Springs, Micro-Actuators

1.0 INTRODUCTION

LIGA-MEMS devices were used as a part of the Defense Advanced Research Projects Agency- Defense Sciences Office (DARPA-DSO) program: Active Material for Photonic System (AMPS). In support of specific LIGA-MEMS device design selection direct mechanical characterization of LIGA-MEMS devices and subcomponents had to be performed. The characterization method described was designed to be an efficient, cost-effective method to support design.

The many LIGA-MEMS devices are too difficult to mechanically characterize because the MEMS device has to interface mechanically with the measurement device. This mechanical interaction is difficult due to the very small sizes of the devices encountered and the limited working spaces available for electrical and mechanical probes under the confines of a high power microscope. It would also be desirable to access the devices without dicing off the parent wafer. What we describe herein is a low cost, accurate force and displacement measurement station. The force measurement is based on using a calibrated cantilevered beam made from an optical fiber.

2.0 EXPERIMENTAL CONSIDERATIONS

In order to develop a method to measure the force an displacement behavior of LIGA-MEMS the specific attributes devices must be considered. These attributes include: device geometry, material anticipated force and displacement behavior. The heights of LIGA-MEMS structures may be on the order of 20 to 200 microns with planar dimensions ranging from 10's of microns to millimeters. The estimated forces required to deflect the structures range from 10 to 10mN. The anticipate deflections range from 10 to 100's of microns.

Passive and active devices were studied. Measurement of passive devices envolved deflecting the device a known amount with a calibrated mechanical probe. Mesurement of active devices involved energizing the active device, measuring displacement produced and then measuring the force by using the cablibrate probe to initially move the device towards the renergized position.

2.1 Displacement Measurement

The displacement measurement of a LIGA-MEMS device is straightforward. A high power optical light microscope, such as shown in Figure 1, is used. The device is mounted to the microscope stage. The microscope stage is a two linear axes, one rotational axis stage. The device is positioned at a point within the field of view, typically aligned with cross-hairs in the microscope eyepiece. The measurement displacement of active or passive device structures may be performed by moving the device along one of the stages linear axes and measuring the distance the stage has traveled from are initial zero point. The

distance may be measured either by using vernier or micrometers scales on the stage or by using a graduated microscope eyepiece. Vernier scales on the stage give a value within +/- 1 micron typically.

For out of plane displacement, the objective can be refocussed on the structure. The change in the plane of focus is measured using a venier scale on the objective focusing system. This plane of focus approach results in a value within +/- 2 microns typically.

2.2 Force measurement

The direct measurement of forces resulting from actuators and spring is difficult to obtain due to the small size of the MEMS devices and their proximity to the surface. Direct force measure requires mechanical interaction of the measurement probe with the MEMS device (1). A few papers have been written for direct measurement of the Young's modulus (2,3). Many papers have been written to characterize the spring constants and, therefore, the force of a cantilevered beam by looking at the resonant frequency of the beam. Once the resonant frequency is obtained the spring constant is computed (4). This requires a prior knowledge of the material properties, and an assumption of the dimensions (design vs. actual). In addition, one assumes an ideal text book structure. For many designs the resonant frequency cannot be obtained because of complex linkages, friction, dampening, and off axis resonances. In our case we had several static models of actuators and springs and processed several iterations on these basic components. What we needed was a method to apply a small calibrated force probe to a MEMS device, in our case LIGA-MEMS, and do it under the close confines of a high power microscope.

3. FIBEROPTIC PROBE

What we propose is the use of a simple, calibrated cantilevered beam made from pure silica SiO_2, a well characterized material. The beam is made from commonly available optical telecommunication fiber. This provides a long and slender rod that can be held at a distance and still probe a device under test. In addition, the fiberoptic tip can be easily melted and shaped (hook or point) such that it can access hard to get at devices in the middle of a wafer.

Telecommunication fiberoptic is a excellent choice due to the tolerances required by the industry. Since the optical loss is highly dependent on the quality of the fiber material, the batch to batch fiber material uniformity is only matched by the semiconductor wafer industry. Therefore, we have a manufacturing process that produces kilometers of fiber of the same diameter and material. The diameter of the single mode fiber has to be maintained to micron tolerances so as to fit into the fiberoptic connector and ferrules. These requirements have driven the manufacturing process such that the uniformity of a fiberoptic is to within a 1% of diameter from batch to batch. For this particular application where small sections of fiber are used the uniformity is much less than 1%. Degradation of the fused silica happens when the pure silica is exposed to moisture. Therefore, to maintain long-term repeatability the fiber has to be hermetically jacketed. The jacket material used for the fiberoptic probes described here was a high temperature polyimide. There are other hermetic materials that are strongly recommended due to their inherent hermeticity. Spectran makes a fiberoptic with Carbon Pyrocoat ®, and Fiberguide Industries makes aluminum coated fibers. These coatings provide a chemical bond with the silica and prevent water induced damage to the fiber.

The fiberoptic probe of a given length has to be held very rigidly to get the ideal boundary condition at the base. A very hard construction epoxy was used to mount the fiber inside steel tubing. A selection of probes were produced to provide a range of force properties. A block with hole and set screw was made to allow for quick change out of fiberoptic probes.

Some devices to be tested, specifically surface micromachined devices, have a very low profile (<10 μm) which a round 140 μm diameter fiber would roll over. This problem can be overcome by tailoring the tip of the fiber with a fiberoptic fusion splicer. See Figure 2. This allows one to create hook and points that protrude from the shank of the fiber.

3.1 Simple Beam Theory

The Force versus deflection for a Fiberoptic cantilevered beam can be simply described with the following equation (5, 6).

$$F = \frac{\delta \cdot 3 \cdot E_S I_T}{(L)^3} \cdot 10^6 \quad \text{micro newtons}$$

Where L is the length of the cantilevered beam, δ is the tip deflection in meters, and E_s and I_T are the modulus of elasticity for fused silica and moment of inertia for the transformed beam. Where I_T for the composite beam is (refer to strength of) (Materials text if appropriate):

$$I_T = \frac{(EI)_{silica} + (EI)_{polyimide}}{E_{Silica}} \quad \text{Where: } (EI)_{Polyimide} = E\left(I_{\substack{outer \\ radius}} - I_{\substack{inner \\ radius}}\right)$$

and

$$I := \frac{\pi \cdot R^4}{4}$$

Where E_s for Fused silica is 73 GPa (6) and the E for polyimide is nominally 3.2 GPa. The effect from the jacket material is a small percentage of the effective silica beam stiffness, $E_s I_s$. In our case the fibers that we used were 140/125 and 275/240 μm jacket /glass diameter polyimide coated fiberoptics. The polyimide only adds ≅3% to the total Beam stiffness. In Table 1 some off-the-shelf fibers and the associated parameters are listed:

Poly coated Fiber	EI Glass ($N^* m^2$)	EI Polyimide ($N^* m^2$)	Total ($N^* m^2$)
140 J /125-G	8.75^*10^{-7}	2.2^*10^{-8}	8.97^*10^{-7}
275-J/240-G	$11.89 * 10^{-6}$	$3.8^* 10^{-6}$	12.3^*10^{-6}
750-J/720-G	$9.63 * 10^{-4}$	7.5^*10^{-6}	9.70^*10^{-4}

Table 1 Calculated Beam Stiffness of sample fiberoptic diameters

3.2 Calibration

The predicted beam stiffness was verified by empirically measuring the amount of force the tip of the fiber exerted while its base was displaced. The set-up for this is shown in Figure 3, in which a precision scale with an accuracy of +/- 4.9 μN is used to measure the force, and a precision stage with micrometer readout was used to measure the displacement of the base. The resulting curve for the 275/240 polyimide coated fiberoptic is shown in Figure 4. (The EI value for the fiber beam can be calculated using the measured force and displacement values by rearranging equation(1).) A calculated EI

value for the fiber beam was 12.2 X 10^{-6} N*m^2 which agrees well with the predicted value shown in Table 1.

3.3 Dynamic Range

The Dynamic range of this system is fixed by the resolution to which one can measure the deflection of the device under test. A typical dynamic range for this method is approximately 2 orders of magnitude. The upper end of the range is limited by the fiberoptic beam tip deflection. The deflection of the end should not exceed 15 % of the length so as to stay in the linear region where the simple beam theory is accurate. In addition, as the fiber is bent passed this point during the application of force to the device it will begin to slip over the part or entirely off the part. When this is encountered the fiberoptic length should be shortened to get a stiffer beam.

4. FORCE MEASUREMENT PROCEDURE

As shown in Figure 5, the measurement of force involves the accurate measurement of the fiberoptic probe base deflection and movement of the spring or actuator to which the fiberoptic is being applied. This setup has two decoupled stages. The stage that holds the fiberoptic is moved by a stepper motor with an integrated vernier with 0.39 micron readout resolution. The device is mounted and can be powered on the stage under the microscope. The microscope stages have magnetic strip verniers which are read to a resolution of 1 micron. The force measurement procedure for passive devices is as follows:

1. Align one edge of the structure under cross-hair of optical microscope. Zero the vernier readout.
2. Using microscope stage, displace structure a selected amount (e.g. 50 μm) relative to the cross hairs.
3. Using the fiberoptic probe stage, bring fiberoptic probe tip in contact with the structure to be measured. Zero the fiberoptic stage vernier readout.
4. Move fiberoptic stage, thus pushing on the structure, until the edge of the structure is aligned under the optic microscope cross hairs.
5. Measure and record the fiberoptic stage deflection. Calculate the tip deflection of the fiber optic probe. tip deflection = base deflection - structural deflection.
6. Obtain the force applied to the structure from the calibration of the fiberoptic probe.

The results obtained for several LIGA springs are shown in Figure 6.

The procedure for measuring active LIGA devices (e.g. actuators) is similar to the spring but as the actuator is powered its stiffness changes. One must determine the force the actuator can provide at different actuation powers. For the particular LIGA-MEMS thermal actuator which was measured with this force measurement probe, there was a limit to how much deflection could be performed before buckling. Therefore, a small displacement of 5 microns in the direction opposite that of the actuator movement was used to measure the force that an actuator can exert at different power levels. A plot of the displacement and force curve for this actuator is shown in Figure 7.

5. AUTOMATION

Both the device and the fiberoptic probe are on translation stages that can be motorized and controlled via a computer. With the use of image recognition software configuration of an automatic test station can be easily implemented utilizing the fiberoptic probes.

6. CONCLUSIONS

We have demonstrated an inexpensive method for measuring both force and deflection at the same time using commonly available laboratory equipment. We have demonstrated the direct and accurate measurement of force using inexpensive telecommunication fiber

as the basis for a force measurement probe. The results will be used in design and analysis of future LIGA MEMS devices.

7. FUTURE WORK AND RECOMMENDATIONS

In order to refine the measurements described and make this a routine method for mechanical characterization of MEMS and LIGA-MEMS the following need to be realized.

1. NIST traceable standard probes and methods for probe calibration
2. NIST traceable 3-D structures for dimensional/displacement measurement for use in calibration of equipment and instruments
3. NIST provided direction for calibrated methods for independent measurement of LIGA-MEMS structures.

8. ACKNOWLEDGMENTS

This work was supported under the DARPA-DSO contract # DAAH04-95-C-0007. We would also like to thank Dr. Howard Last of the Naval Surface Warfare Center (NSWC) and Dr. John Prater of Army Research Office (ARO) for their comments and suggestions.

9. REFERENCES

1. M. Kohn, "Mechanical Characterization of Shape Memory Micromaterials", 1996, SPIE Vol. 2880-09, p 108-118
2. T. Read, " Measurement of fracture strength and Young's modules of surface-micromachined polysilicon", 1996, SPIE Vol 2880-04, p. 56-63
3. W.N. Sharpe, "New test structures and techniques for measurement of mechanical properties of MEMS materials SPIE Vol. 2880-06, p.78-91
4. Scott A. Miller, "Micromechanical Cantilevers and Scanning Probe Microscopes" , 1995 SPIE Vol 2640-05, p. 45 - 52.
5. F.P. Beer and E.R. Johnston, Jr. , "Mechanics of Materials", 1981, McGraw-Hill
6. W.D. Pilkey and O.H. Pilkey, "Mechanics of Solids" 1974 Quantum Publishers
7. K. E. Petersen, "Silicon as a Mechanical Material", IEEE, Vol. 70, No 5 May 1982

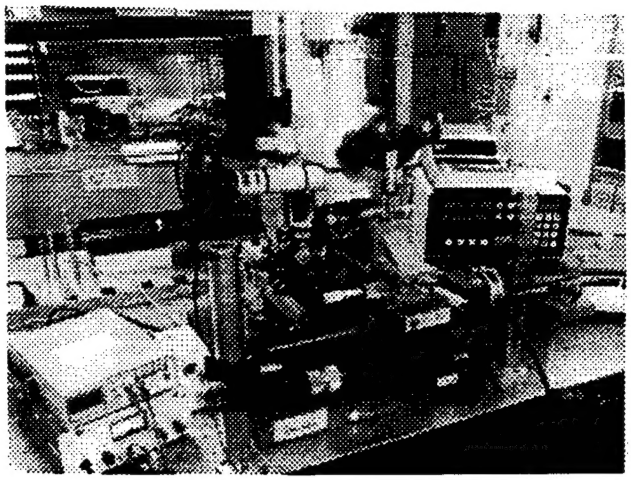

Figure 1. Picture of force and displacement characterization

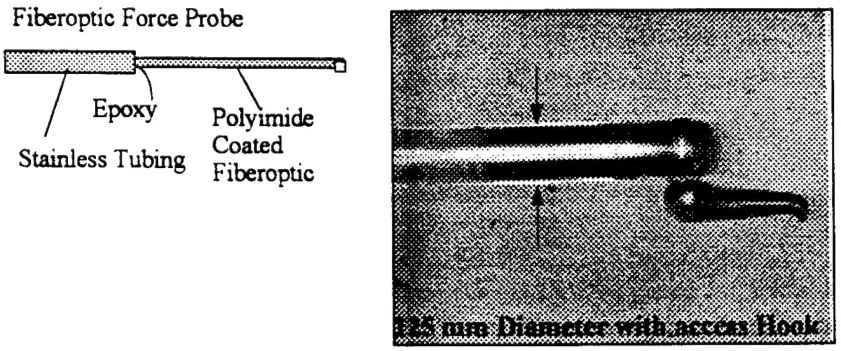

Figure 2 Picture of fiberoptic Probe (Artist) and actual probe with special tip

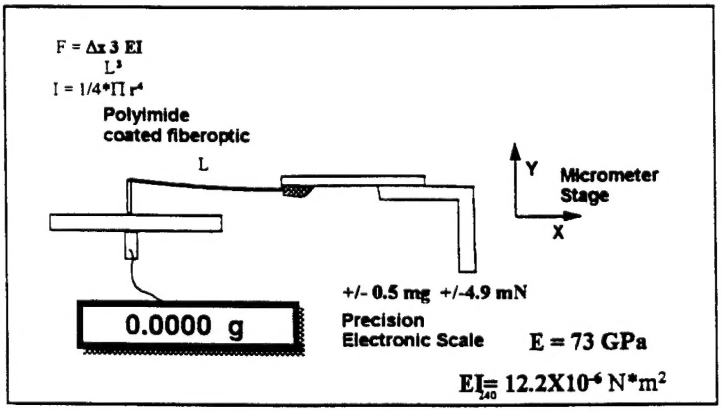

Figure 3 Graphical description of fiberoptic probe calibration setup

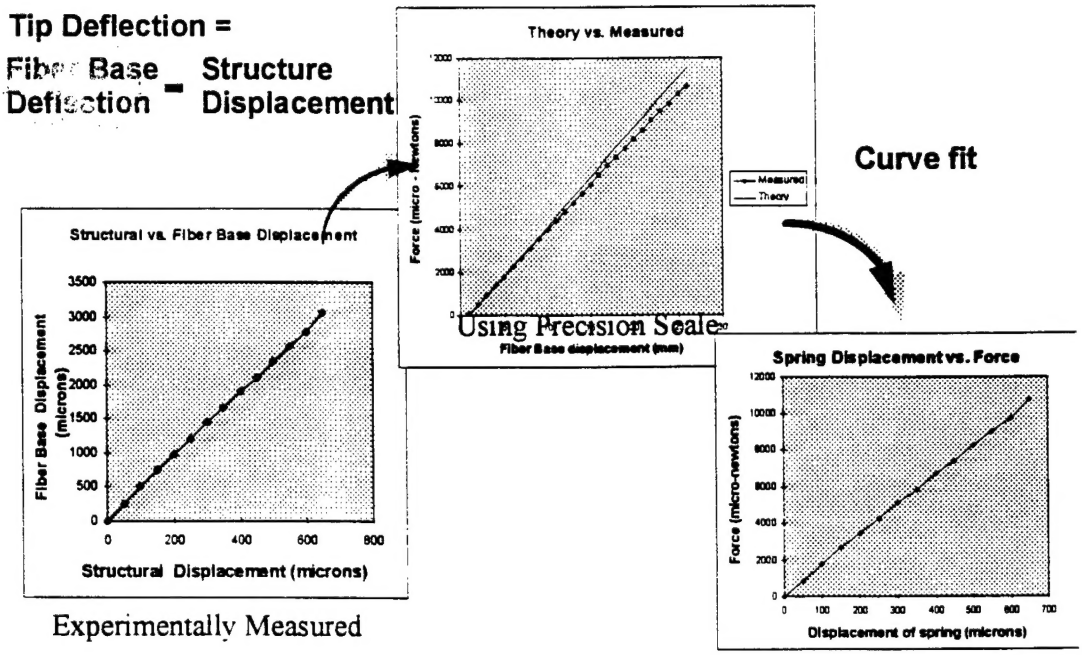

Figure 4 Schematic illustration of procedure to obtain Force vs displacement for structures

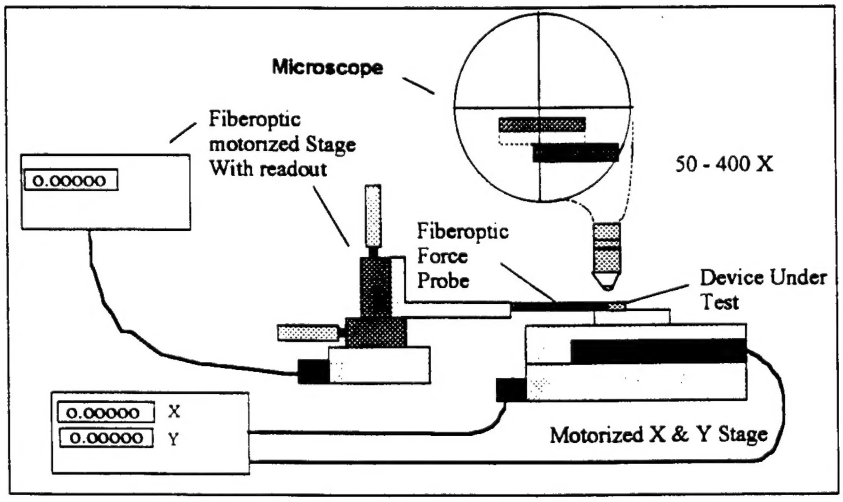

Figure 5 Graphical Description of force/displacement characterization station

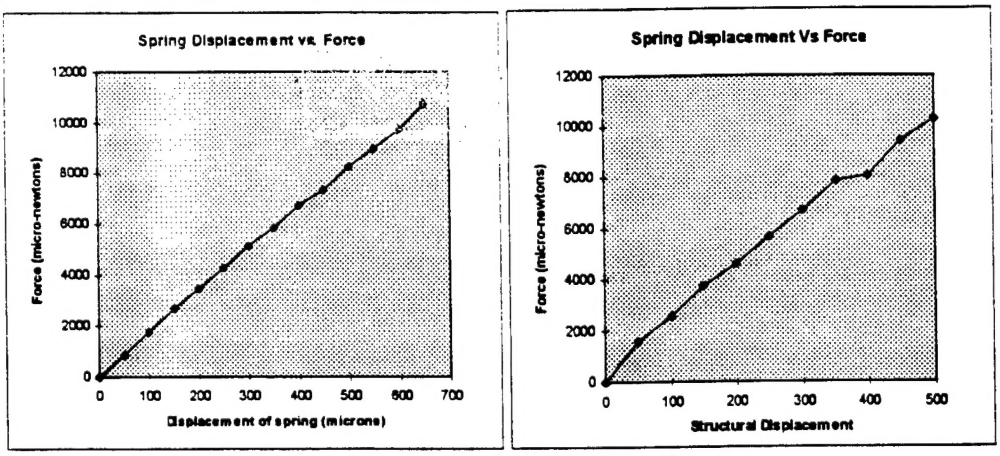

* NSWC Navel Surface Warfare Center

Figure 6 Measured force vs displacement of NSWC springs

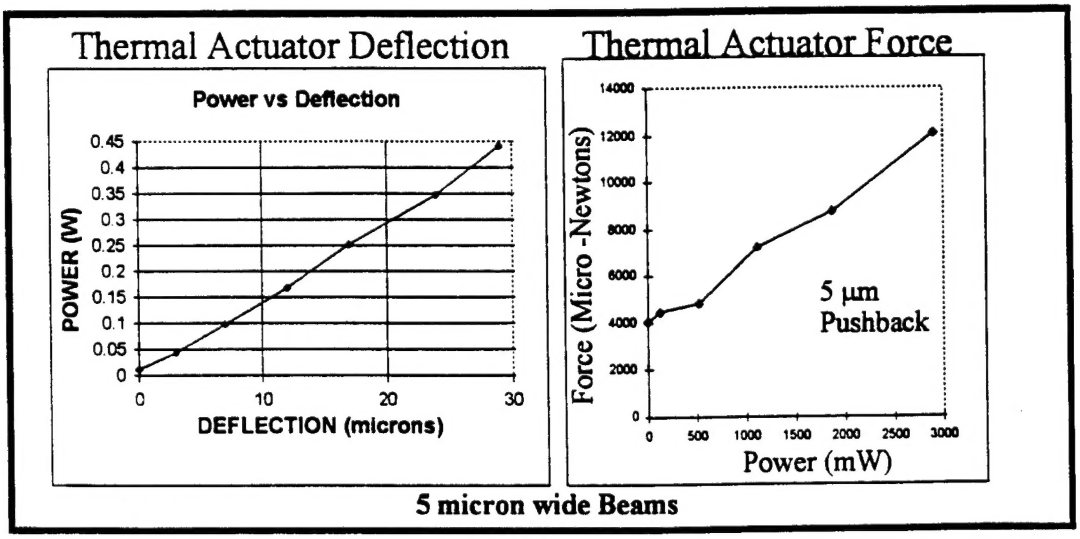

Figure 7 Thermal actuator Force / Deflection versus Power characterization curves